RESPONSE TO REQUEST FOR ADDITIONAL INFORMATION

05/31/2013

US-APWR Design Certification

Mitsubishi Heavy Industries

Docket No. 52-021

RAI NO.:	**NO. 909-6315 REVISION 3**
SRP SECTION:	**03.07.02 - SEISMIC SYSTEM ANALYSIS**
APPLICATION SECTION:	**3.7.2**
DATE OF RAI ISSUE:	**03/05/2012**

QUESTION NO.: 03.07.02-188

In Section 2.3.2.1 of MUAP-11002(R1), "Consideration of Concrete Cracking Effects," (Page 24), the last sentence states, "Therefore, no attempt to characterize the response of a more rigid, concrete foundation is deemed necessary."

The staff notices that this approach is inconsistent with that used in Subsection 4.5.1 of MUAP-10001 (R4), in which two analyses are performed. One analysis assumes that the concrete is cracked, and the other analysis assumes that the concrete is not cracked. The responses obtained from these two analyses are then enveloped to develop the basis for the seismic analyses and design. The Applicant is requested to provide a rationale for not using a similar dual approach for the T/B analyses, and, also, to provide numerical data that shows that the approach taken in MUAP-11002(R1) is conservative.

ANSWER:

This answer revises and replaces the previous MHI answer that was transmitted by letter UAP-HF-12124 of June 5, 2012 (ML12158A478)

The design of the T/B structures was modified as part of the comprehensive Seismic Closure Plan (UAP-HF-13034, 2/15/2013) and documented in the TeR MUAP-11002 (Rev. 2).

The last sentence of Subsection 2.3.2-1 of MUAP-11002 (Rev. 1) has been removed from TeR MUAP-11002 (Rev. 2).

SSI analyses have been performed that consider the effects of uncracked substructure concrete conditions on the superstructure. Technical Report MUAP-11002 (Rev. 3) will include Appendix A to present the results regarding the uncracked concrete analysis for the T/B complex. Appropriate sections of the TeR will also be revised to include the results of Appendix A.

Minimum factors of safety against seismic overturning for each soil profile for both the east-west and north-south directions for the uncracked condition have been calculated and will be reported in Appendix A of the TeR. Maximum seismic bearing pressures and minimum contact area ratios for each soil profile for the uncracked condition have been calculated and will be reported in Appendix A of the TeR. The stability evaluations of the results of those uncracked analyses will be discussed in the MUAP-11002 (Rev. 3), in subsections 6.2 and 6.4.

Impact on DCD

There is no impact on the DCD

Impact on R-COLA

There is no impact on the R-COLA.

Impact on PRA

There is no impact on the PRA.

Impact on Topical Report / Technical Report

The following Subsections in MUAP-11002 will be revised as indicated in Attachment 1 of this response:

2.2

2.3.2.1

4.3.2

4.3.3

Table 4.3.3-3

6.2

6.4

7.0

Appendix A will be added to MUAP-11002 as indicated in Attachment 2 of this response to address the uncracked substructure SSI results.

This completes MHI's response to the NRC's question.

ATTACHMENT 1

2.0 METHODOLOGY FOR DEVELOPMENT OF T/B COMPLEX FE MODELS

The three-dimensional (3-D) fine and coarse mesh Finite Element (FE) models of the T/B and Electrical Room structures were developed using the GT STRUDL and ANSYS software packages. The T/G Pedestal model LMSM was generated in ANSYS. Historically, the fine mesh model was developed for use in reinforced concrete structural design using GT STRUDL. The coarse mesh GT STRUDL model was developed from the fine mesh GT STRUDL model and used for the ACS SASSI SSI model. Due to limitations of GT STRUDL Version 31, the fine mesh model could only be analyzed up to a frequency of 21 Hz. To overcome this limitation, the fine and coarse mesh models were subsequently developed and analyzed using ANSYS. The coarse mesh T/B and Electrical Room model was validated against the fine mesh model in ANSYS. Validation of the models is discussed in Section 3.0 of this report.

The ACS SASSI T/B complex model was then generated by combining the ANSYS T/B and Electrical Room coarse mesh model with the ANSYS T/G Pedestal LMSM model.

2.1 Structural Geometry

Figures 1.1-2 and 1.1-3 show the elevation view looking south and elevation view looking north, respectively, of the T/B complex structures for the combined coarse mesh ACS SASSI model. Overall dimensions, top of floor elevation and actual seismic weight for each floor for the T/B superstructure are provided in Table 2.1-1. Overall dimensions, top of floor elevation and actual seismic weight for each floor for the Electrical Room superstructure are provided in Table 2.1-2.

A 3-D view of the T/B and Electrical Room substructure is shown on Figure 2.1-1. Figure 2.1-2 shows a 3-D view of the substructure with the T/B first floor slab removed. Overall dimensions for the T/B and Electrical Room substructure are listed in Table 2.1-3.

2.2 Material Properties

The T/B and Electrical Room superstructures are braced steel frames consisting of structural steel with the following properties:

- Young's Modulus, E = 4.176 x 10^6 kips per square foot
- Poisson's Ratio = 0.3
- ~~Damping Value = 4 percent~~
- Unit Weight = 0.49 kips per cubic foot
- Specified minimum yield stress, F_y = 50 kips per square inch (American Society for Testing and Materials (ASTM) A992 for wide-flange shapes)
- Specified minimum yield stress, F_y = 50 kips per square inch (ASTM A572 for built-up plate members for plates up to and including 4 inches thick)

- Specified minimum yield stress, F_y = 42 kips per square inch (ASTM A572 for built-up plate members for plates up to and including 6 inches thick)

The T/B and Electrical Room substructure and the T/G Pedestal basemat consist of normal weight, reinforced concrete material. The reinforced concrete has the following properties:

- Compressive Strength of Concrete, f'_c = 4,000 pounds per square inch
- Young's Modulus for Uncracked Concrete, $E_{uncracked}$ = 5.18 x 10^5 kips per square foot (See Subsection 2.3.2.1)
- Young's Modulus for Cracked Concrete, $E_{cracked}$ = 2.59 x 10^5 kips per square foot (See Subsection 2.3.2.1)
- Poisson's Ratio = 0.17
- ~~Damping Value = 4 percent~~
- Unit Weight = 0.15 kips per cubic foot

For the uncracked concrete models, the three percent material damping was used for both concrete and steel material. Four percent material damping was used for concrete and steel material for the cracked concrete models.

2.3 GT STRUDL Models Development

2.3.1 Structural Discretization and Finite Element (FE) Types

In the GT STRUDL models, the structures are modeled with north as the positive global Y-axis, east as the positive global X-axis and upward as the positive global Z-Axis. The origin of the coordinate system is at the intersection point of column rows AT and 1T (refer to Figure 1.1-1). The coordinate system and the location for the origin of the coordinate system are also the same for the ACS SASSI and ANSYS models.

The T/B and Electrical Room superstructure models are developed by establishing nodes at the steel connections. The steel beams, girders, horizontal and vertical bracing, and columns are modeled as linear beam elements between the nodes.

The T/B and Electrical Room substructure model includes a combination of shell and solid block elements representing the structural walls, slabs, basemat, and massive concrete, and linear elements representing beams and columns. The condensate pump foundation is a mass concrete structure with pipe and pump can openings. The condensate pump foundation is modeled with solid block elements. At the interfaces of the shell elements and solid block elements, the shell elements are extended one row into solid elements, and share common nodes with the solid elements. The material density of these shell elements is zero. This modeling approach enables transfer of moments between shell elements and solid block elements. The walls are modeled such that the shell element center planes are located approximately at the centerline of the actual structure.

2.3.2 Modeling of Dynamic Stiffness

2.3.2.1 Consideration of Concrete Cracking Effects

In the body of this report, the stiffness of the concrete substructure is considered ~~only~~ based on reduced (cracked concrete) stiffness. In accordance with the methodology in Subsection 2.4.2.1 of MUAP-10006 (Reference 6) for consideration of concrete cracking in the analyses of the US-APWR Seismic Category I structures, the SSI analysis of the T/B complex considers reduced (cracked concrete) stiffness as 50 percent of the nominal uncracked stiffness of the reinforced concrete members.

Appendix A of this report, provides additional SSI analysis results based on the uncracked stiffness of the substructure.

2.3.2.2 Structural Openings

All major openings in the T/B substructure walls are generated in the GT STRUDL FE model, and therefore no stiffness adjustment is required for openings.

2.3.3 Equivalent Dynamic Mass

The inertial properties include all tributary mass expected to be present at the time of the SSE. The equivalent seismic mass includes:

- The mass of all of the structural elements
- The mass of permanent equipment
- The mass equivalent of a superimposed dead load of 50 pounds per square foot to account for minor equipment, piping and cable raceways
- 25 percent of the floor design live load
- 75 percent of the roof design snow load

2.3.4 Modeling of Equipment

Equipment stiffness is not explicitly simulated in the model. The equipment mass is applied over a representative floor area in the model. This is in accordance with the procedure specified in NUREG-0800 SRP 3.7.2 (Reference 2), Subsection 3.7.2.II.3D.

2.3.5 Fine Mesh Substructure Model

The T/B and Electrical Room fine mesh GT STRUDL substructure model was used for structural analysis and foundation design.

- Obtain the maximum relative displacement for each subsurface profile from the combined displacement time histories. To consider that the input motions may reverse direction, the maximum relative displacements were developed as the absolute value of the maximum positive displacement (moving toward) and minimum negative displacement (moving away) of the combined displacement time history. The maximum displacement toward the R/B complex of each T/B and Electrical Room node relative to the free-field is the enveloped value of the maximum relative displacements from each of the six generic subsurface profiles.

4.3.2 Results of Acceleration Transfer Functions

Prior to computing the T/B and Electrical Room node displacements, acceleration transfer functions were plotted for the selected nodes and reviewed to confirm that the number of frequencies included in the SSI analyses were sufficient to develop acceptable interpolated acceleration transfer functions. For the cracked substructure condition, Figures 4.3.2-1 through 4.3.2-20 show the TFU amplitudes for discrete frequencies where ACS SASSI calculated the amplitudes, and the TFI amplitudes. The TFI amplitude line was developed by interpolation between the TFU values. Figures 4.3.2-1 through 4.3.2-10 show the TFU and TFI amplitude plots for the Y direction (North-South) due to Y direction ground motion for five of the 27 selected nodes at the north T/B complex wall located nearest to the R/B complex. Figures 4.3.2-11 through 4.3.2-20 show the TFI and TFU amplitude plots for the X direction (East-West) due to X direction ground motion for five of the 35 nodes on the T/B and the Electrical Room adjacent walls. Appendix A contains the results based on the uncracked substructure condition.

Figures 4.3.2-1 through 4.3.2-20 also show that there is good agreement between the trend of the TFI and the TFU values at each SSI frequency, which indicates that sufficient frequencies were included in the SSI analysis to appropriately represent the acceleration transfer functions. The TFI and the TFU for the remaining nodes that are not shown have similar levels of agreement.

Figures 4.3.2-21 through 4.3.2-25 show the TFI in the Y direction (North-South) due to Y direction ground motion for the six subsurface profiles for five of the 27 nodes at the north T/B complex wall located nearest to the R/B complex. Figures 4.3.2-26 through 4.3.2-30 show the TFI in the X direction (East-West) due to X direction ground motion for the six subsurface profiles for five of the 35 nodes on the T/B and Electrical Room adjacent walls. The comparison shows that under SSI effects, the dominant frequencies shift to lower frequencies as the stiffness of the subsurface profile decreases.

4.3.3 Results of Maximum T/B Complex Displacements

Tables 4.3.3-1 and 4.3.3-2 report the SSI computed maximum relative T/B complex displacements in the X (East-West) and Y (North-South) directions at the 66 T/B and Electrical Room nodes with respect to the free-field input ground surface motion for the six subsurface profiles. Appendix A contains the results based on the uncracked substructure condition.

For the selected nodes adjacent to the R/B complex (Figure 4.3-1), the maximum displacements in the Y-direction (North-South) range from 0.~~1006~~0760 inch at node 290 to 2.~~3210~~3784 inches at node

605 (Tables 4.43.3-2 and A.3-2). These values represent an envelope of both the cracked and uncracked substructure conditions. For the cracked and uncracked substructure condition and each of the 66 selected nodes, Table 4.3.3-3 shows the subsurface profile associated with the computed maximum relative X and Y direction displacements with respect to free-field motion.

Table 4.3.3-3 Summary of Governing Subsurface Profiles for Maximum Relative Displacement in X (East-West) and Y Direction (North-South) Directions

(Sheet 1 of 3)

Node Number	Elevation (Feet)	Governing Subsurface Profile			
		Cracked Substructure		Uncracked Substructure	
		East-West Direction	North-South Direction	East-West Direction	North-South Direction
290	2.75	270-200	270-200	270-200	270-500
338	2.75	270-200	270-200	270-200	270-200
386	2.75	270-200	270-200	270-200	270-200
389	2.75	270-200	270-200	270-200	270-200
392	2.75	270-200	270-200	270-200	270-200
395	2.75	270-200	270-200	270-200	270-500
398	2.75	270-200	270-200	270-200	270-500
401	2.75	270-200	270-500	270-200	270-500
473	2.75	270-200	270-200	270-200	270-200
560	2.75	270-200	270-200	270-200	270-500
676	2.75	270-200	270-200	270-200	270-500
792	2.75	270-200	270-200	270-200	270-500
879	2.75	270-200	270-200	270-200	270-500
908	2.75	270-200	270-200	270-500	270-200
911	2.75	270-200	270-200	270-200	270-200
914	2.75	270-200	270-200	270-200	270-200
917	2.75	270-200	270-200	270-200	270-500
920	2.75	270-200	270-200	270-200	270-500
923	2.75	270-200	270-200	270-200	270-500
544	24.75	900-100	270-200	900-100	560-500
606	24.75	900-100	900-200	900-100	900-200
627	24.75	900-100	900-200	900-100	900-100
630	24.75	900-100	900-200	900-100	900-100
633	24.75	900-100	560-500	900-100	900-100
636	24.75	900-100	270-200	900-100	560-500
4965	24.75	900-200	2032-100	900-200	900-200
4968	24.75	900-200	2032-100	900-200	2032-100
5035	24.75	900-200	2032-100	900-200	2032-100

Table 4.3.3-3 Summary of Governing Subsurface Profiles for Maximum Relative Displacement in X (East-West) and Y Direction (North-South) Directions

(Sheet 2 of 3)

Node Number	Elevation (Feet)	Governing Subsurface Profile			
		Cracked Substructure		Uncracked Substructure	
		East-West Direction	North-South Direction	East-West Direction	North-South Direction
570	33.5	270-200	560-500	270-200	560-500
753	33.5	270-200	560-500	560-500	560-500
1411	33.5	270-200	560-500	560-500	560-500
2657	33.5	270-200	560-500	270-200	560-500
2738	33.5	560-500	560-500	560-500	270-200
5039	33.5	560-500	270-500	270-500	270-500
5042	33.5	900-200	270-500	560-500	900-100
5045	33.5	900-200	900-200	900-200	900-100
5048	33.5	900-200	900-200	900-200	900-200
5080	33.5	560-500	2032-100	270-500	900-200
542	60.5	900-200	900-200	900-200	560-500
573	60.5	560-500	900-200	270-200	560-500
605	60.5	900-200	900-200	900-200	900-100
626	60.5	900-200	900-200	560-500	900-100
629	60.5	900-200	900-100	560-500	560-500
632	60.5	900-200	2032-100	560-500	900-200
635	60.5	900-200	900-200	560-500	560-500
755	60.5	560-500	900-200	560-500	560-500
1421	60.5	270-200	900-200	560-500	560-500
2659	60.5	560-500	900-200	2032-100	560-500
2740	60.5	560-500	900-200	560-500	560-500
4964	63.5	270-200	2032-100	270-200	900-200
4967	63.5	270-200	900-200	270-200	2032-100
5034	63.5	270-200	900-200	270-200	900-100
5037	63.5	560-500	900-200	270-500	900-200
5041	63.5	560-500	900-200	900-200	900-100
5044	63.5	900-200	900-200	900-200	900-200
5047	63.5	900-200	900-200	900-200	900-200
5079	63.5	900-200	900-200	900-200	2032-100
574	87.6667	560-500	900-200	560-500	560-500

Table 4.3.3-3 Summary of Governing Subsurface Profiles for Maximum Relative Displacement in X (East-West) and Y Direction (North-South) Directions

(Sheet 3 of 3)

Node Number	Elevation (Feet)	Governing Subsurface Profile			
		Cracked Substructure		Uncracked Substructure	
		East-West Direction	North-South Direction	East-West Direction	North-South Direction
756	87.6667	560-500	900-200	560-500	560-500
1422	87.6667	560-500	900-200	560-500	560-500
2660	87.6667	560-500	900-200	270-200	560-500
2741	87.6667	2032-100	900-200	2032-100	560-500
661	169.417	900-200	900-200	560-500	900-100
745	169.417	900-200	900-200	560-500	900-100
3164	169.417	2032-100	900-200	900-200	900-100
3210	169.417	2032-100	900-200	900-200	560-500

Depending on the rotational directions of the overturning moment, the driving force and moments were moved to the corresponding overturning axis.

The factor of safety against overturning is the ratio of the resisting moment to the overturning moment about the same rotational axis. The smallest factor of safety for all the time steps governs. A factor of safety greater than or equal to 1.1 is required, which is consistent with NUREG-0800 SRP 3.8.5 (Reference 13).

The SSSI overturning stability evaluation methodology is described in Appendix C.

6.2 Overturning Stability Evaluation Results

The minimum overturning factor of safety for each subsurface profile for both the east-west (x-axis) and north-south (y-axis) directions is shown on Table 6.2-1 for the cracked case. Appendix A reports the minimum overturning factor of safety for each subsurface profile for both the east-west (x-axis) and north-south (y-axis) directions in Table A.4-1 for the uncracked case.

The factors of safety for all subsurface profiles for the T/B complex are acceptable as they are all greater than 1.1.

6.3 Bearing Pressure and Contact Area Ratio Evaluation Methodology

The forces and moments involved in bearing pressure calculations are the same as those in the overturning evaluation. In addition, the analysis also considered cases where the buoyancy force was included and cases where it was excluded. The buoyancy force is treated in this manner because buoyancy may increase or decrease the bearing pressure. The buoyancy force increases bearing pressure by decreasing the contact area between the subgrade and foundation and decreases bearing pressure by counteracting downward structure loads.

The T/B and Electrical Room substructure was treated as a rigid body. The base of the substructure was divided into smaller areas with grid lines. A majority of the grid lines were spaced between 4 and 5 feet. Initially, each point at an intersection of grid lines was evaluated and flagged as effective if the point was within the contact area between the foundation and soil or ineffective if the point fell in an opening area or outside the foundation profile. The section properties including center of gravity, area, and moments of inertia were calculated with the tributary areas of the effective points. The stress at each effective point was calculated and the points that had tension stresses were removed from the effective point set.

In the iteration of the bearing pressure calculation, the foundation section properties were recalculated due to changes to the set of effective points. The total forces and moments were moved from the previous center of gravity to the new center of gravity. The stress at each point was calculated, and all points having tension stresses were removed from the effective point set. The iteration was stopped when no tension stress occurred at any point or the remaining points

failed to form a plane, i.e. less than three points were left or all of the remaining points were collinear. In the latter case, the foundation would have been reported as "unstable" with 0 percent contact area ratio, and in the former case, the foundation's maximum bearing pressure and minimum contact area ratio were reported.

The SSSI bearing pressure and contact area ratio evaluation methodology are described in Appendix C.

6.4 Bearing Pressure and Contact Area Ratio Evaluation Results

The maximum bearing pressure and minimum contact area ratio for each soil profile are shown in Table 6.4-1 for the cracked case. Appendix A reports the maximum bearing pressure and minimum contact area ratio for each soil profile in Table A.4-2 for the uncracked case. The results of Table 6.4-1, and Table A.4-2 include cases with and without buoyancy. According to the tables, the maximum bearing pressure is 9.2 kips per square foot and the minimum contact area ratio is 73.4 percent.

6.5 Flotation Evaluation Methodology

The buoyancy force for all the stability analyses, including flotation used the highest groundwater level of one foot below plant grade, which is based on the Table 2.0-1 of the DCD (Reference 1). The factor of safety against flotation was calculated as the ratio between the concrete dead load and the buoyant force on the substructure. A factor of safety greater than or equal to 1.1 is required, in accordance with NUREG-0800 SRP 3.8.5 (Reference 13).

The approach used for determining the minimum factor of safety against flotation was to determine the earliest stage of construction past completion of the T/B and Electrical Room substructure at which the T/B and Electrical Room meets the required minimum factor of safety.

6.6 Flotation Evaluation Results

The minimum factor of safety against flotation for the T/B complex substructure is 1.94. This factor of safety is reached once the T/B and Electrical Room substructure is constructed to the bottom of the first floor slab and the weight of the T/B first floor slab, equipment, and the T/B and Electrical Room superstructure dead loads are all excluded in the resisting force. Since the factor of safety against flotation is greater than 1.1, the flotation stability is adequate for the T/B complex.

7.0 SUMMARY

This TeR documents the methodology, models and results of the T/B complex SSI analyses. Also documented are the structural integrity and stability analyses of the T/B and Electrical Room.

Section 3.0 presents the description and validation of the FE model used for SSI analyses. The dynamic properties of the T/B complex model are presented in Subsections 3.1.2 and 3.1.3. The results of the SSI analyses of the ACS SASSI FE model for six generic subsurface profiles are presented in Subsection 4.3.3.

Section 6.0 presents the evaluation of overturning stability, bearing pressure, and flotation. Results of the overturning stability evaluation are presented in Subsection 6.2 and in Table 6.2-1 and Appendix A, Table A.4-1. Results of the evaluation for dynamic soil bearing pressure beneath the T/B and Electrical Room are presented in Subsection 6.4 and Table 6.4-1 and Appendix A, Table A.4-2. Results of the flotation evaluation are presented in Subsection 6.6.

The results of the T/B complex SSI analyses demonstrate that the Seismic Category II T/B complex maintains its stability and structural integrity during a seismic event such that any impact on Seismic Category I structures is precluded.

ATTACHMENT 2

Appendix A

Uncracked Structure-Soil Interaction Analysis And Stability Evaluation Results

APPENDIX A TABLE OF CONTENTS

LIST OF TABLES

LIST OF FIGURES

A.1.0 INTRODUCTION

This appendix documents the Structure-Soil Interaction (SSI) results and the stability evaluation results of the Turbine Building (T/B) complex based on the uncracked substructure. The three percent material damping is used for both substructure and superstructure. The uncracked results of the SSI analyses and the stability evaluations of the T/B complex are provided for the six generic layered soil profiles: 270-200, 270-500, 560-500, 900-100, 900-200, and 2032-100. The methodology used to develop the SSI analyses results is identical to those discussed in subsection 4.3 of this TeR. The methodology used to develop the stability evaluation results is identical to those discussed in subsections 6.1 and 6.3 of this TeR.

A.2.0 RESULTS OF ACCELERATION TRANSFER FUNCTIONS

Figures A.2-1 through A.2-20 show the TFU amplitudes for discrete frequencies where ACS SASSI calculated the amplitudes, and the TFI amplitudes. The TFI amplitude line was developed by interpolation between the TFU values. Figures A.2-1 through A.2-10 show the TFU and TFI amplitude plots for the Y direction (North-South) due to Y direction ground motion for five of the 27 selected nodes at the north T/B complex wall located nearest to the R/B complex. Figures A.2-11 through A.2-20 show the TFI and TFU amplitude plots for the X direction (East-West) due to X direction ground motion for five of the 35 nodes on the T/B and the Electrical Room adjacent walls.

Figures A.2-1 through A.2-20 also show that there is good agreement between the trend of the TFI and the TFU values at each SSI frequency, which indicates that sufficient frequencies were included in the SSI analysis to appropriately represent the acceleration transfer functions. The TFI and the TFU for the remaining nodes that are not shown have similar levels of agreement.

Figures A.2-21 through A.2-25 show the TFI in the Y direction (North-South) due to Y direction ground motion for the six subsurface profiles for five of the 27 nodes at the north T/B complex wall located nearest to the R/B complex. Figures A.2-26 through A.2-30 show the TFI in the X direction (East-West) due to X direction ground motion for the six subsurface profiles for five of the 35 nodes on the T/B and Electrical Room adjacent walls. The comparison shows that under SSI effects, the dominant frequencies shift to lower frequencies as the stiffness of the subsurface profile decreases.

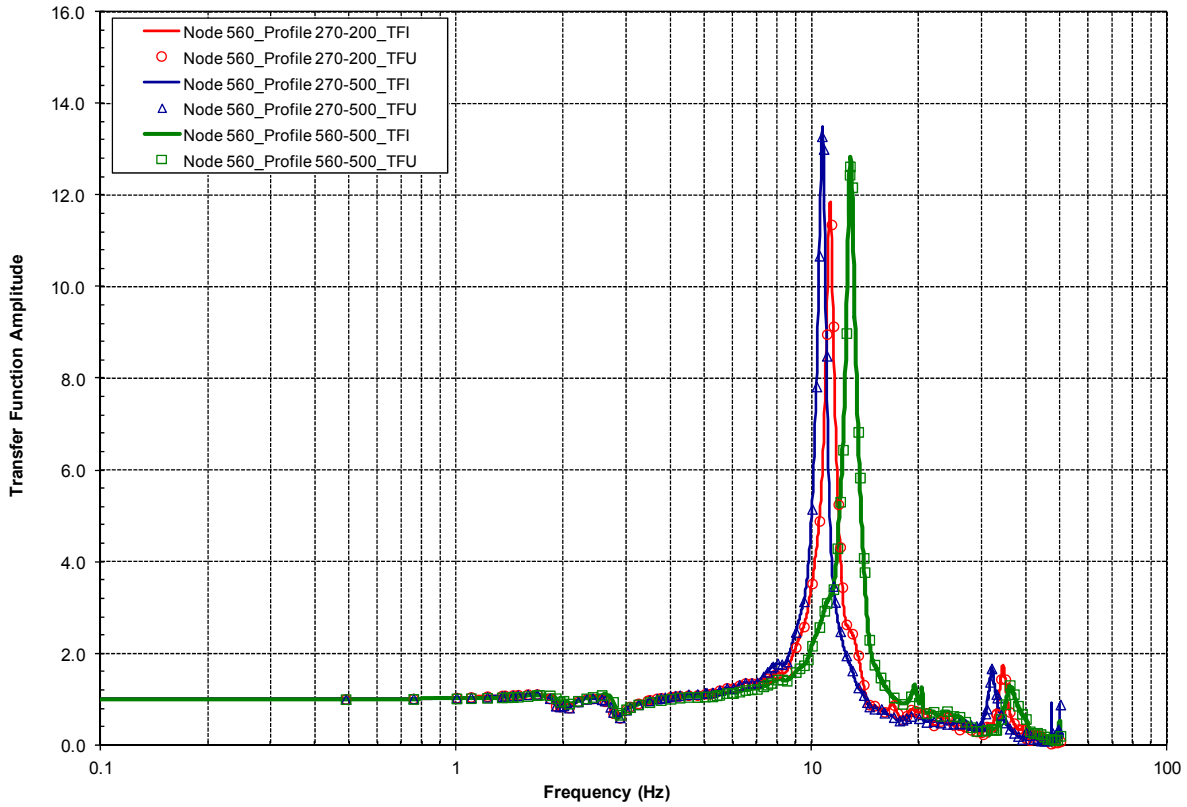

Figure A.2-1 Acceleration Transfer Functions for Subsurface Profiles 270-200, 270-500, and 560-500 for Y Direction (North-South) Due to Y Direction Ground Motion at Node 560

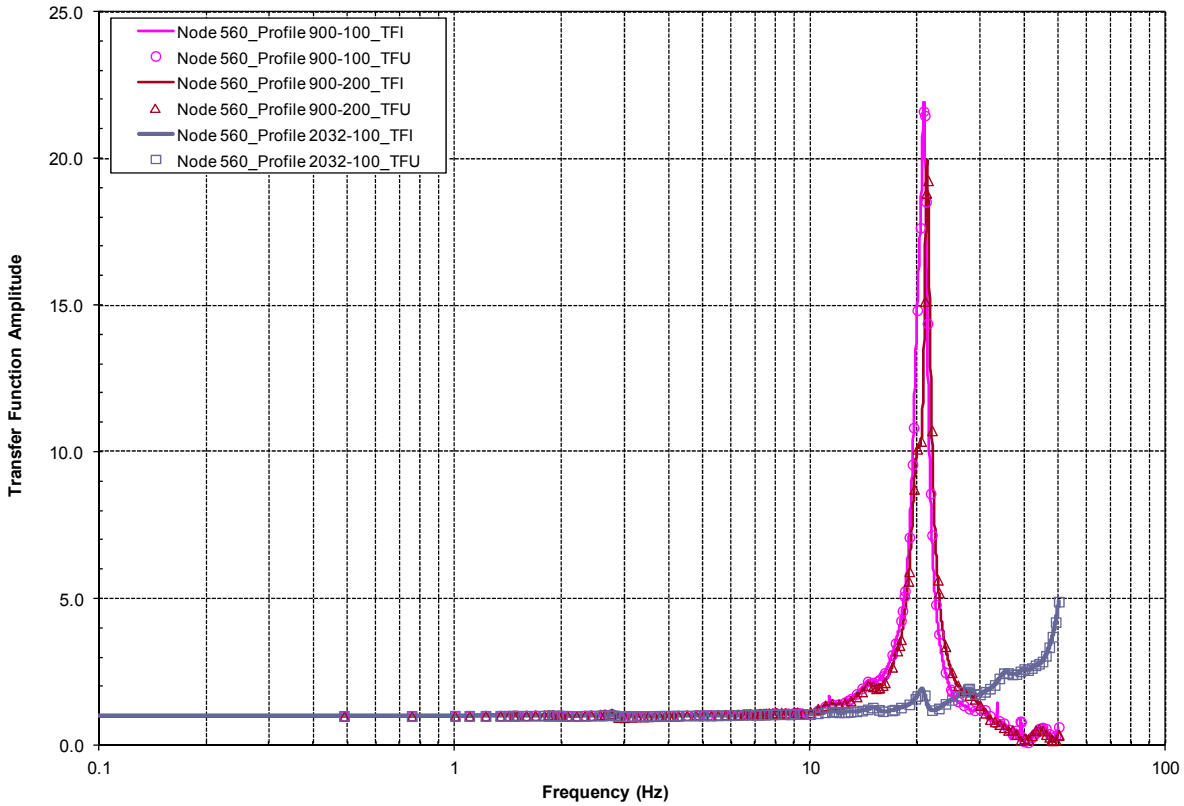

Figure A.2-2 Acceleration Transfer Functions for Subsurface Profiles 900-100 and 900-200, and 2032-100 for Y Direction (North-South) Due to Y Direction Ground Motion at Node 560

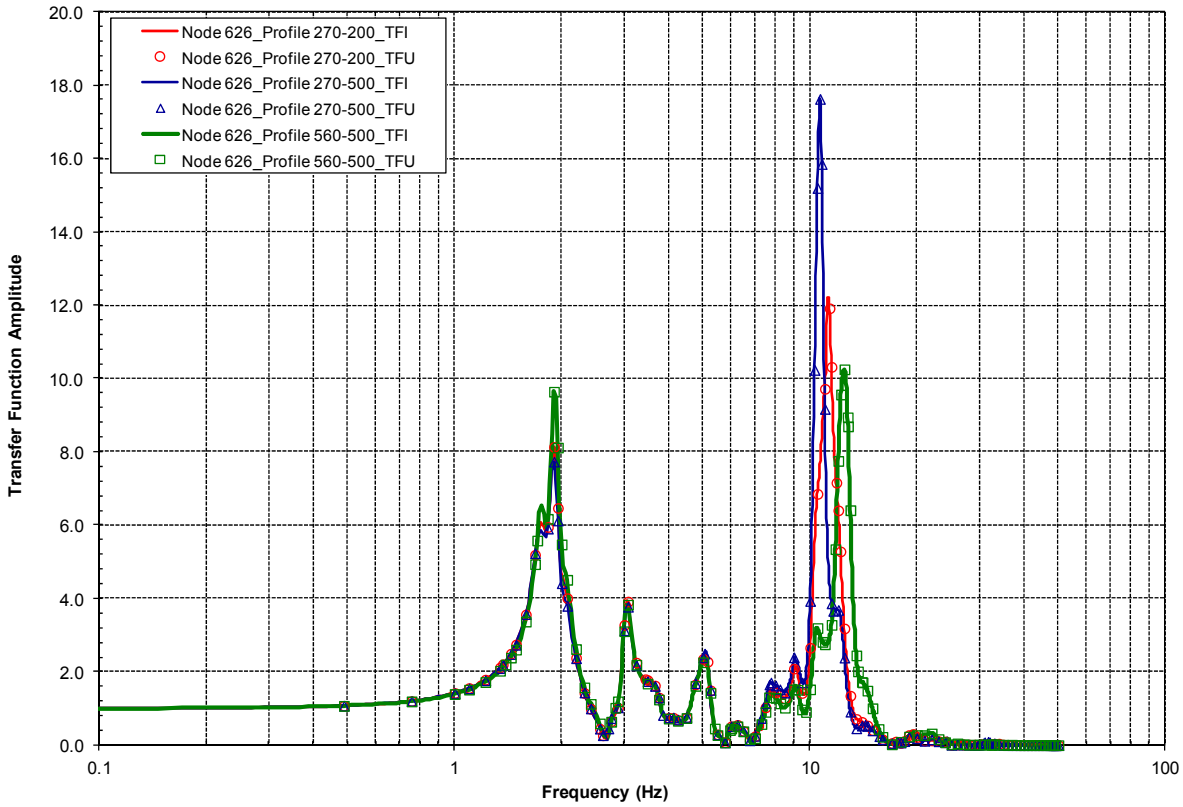

Figure A.2-3 Acceleration Transfer Functions for Subsurface Profiles 270-200, 270-500, and 560-500 for Y Direction (North-South) Due to Y Direction Ground Motion at Node 626

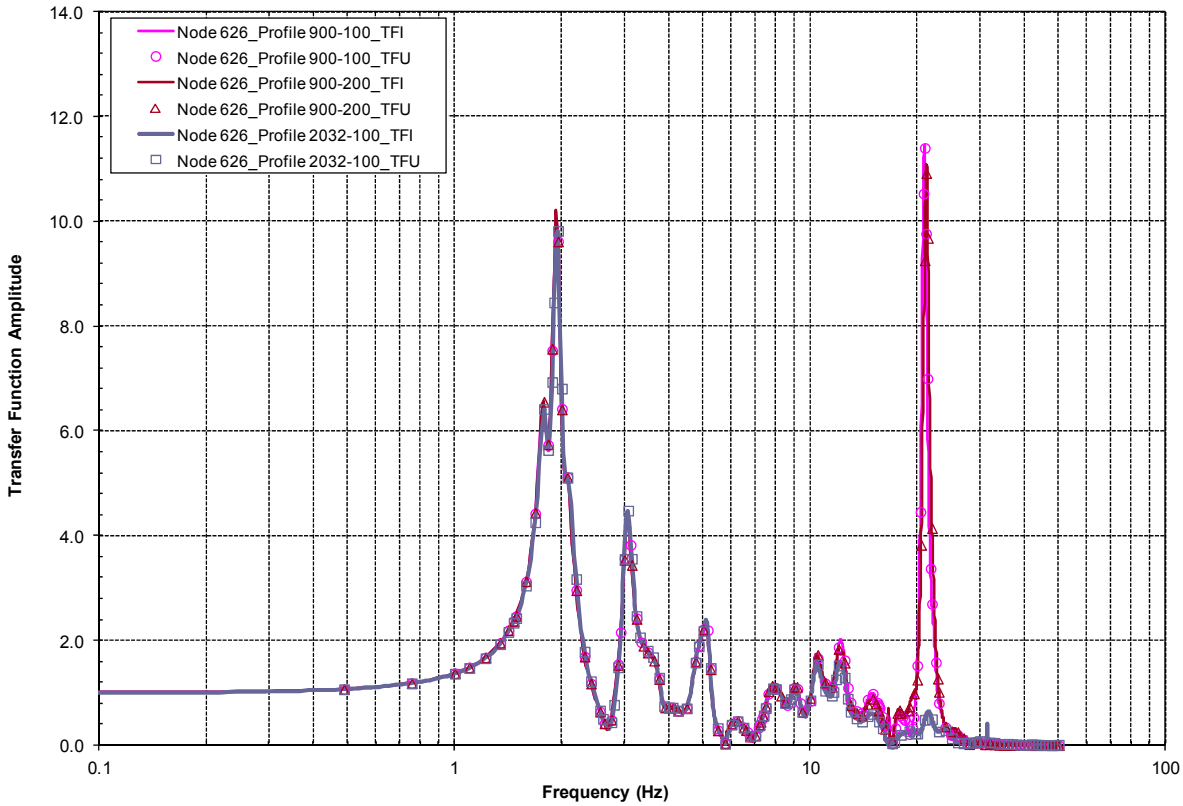

Figure A.2-4 Acceleration Transfer Functions for Subsurface Profiles 900-100 and 900-200, and 2032-100 for Y Direction (North-South) Due to Y Direction Ground Motion at Node 626

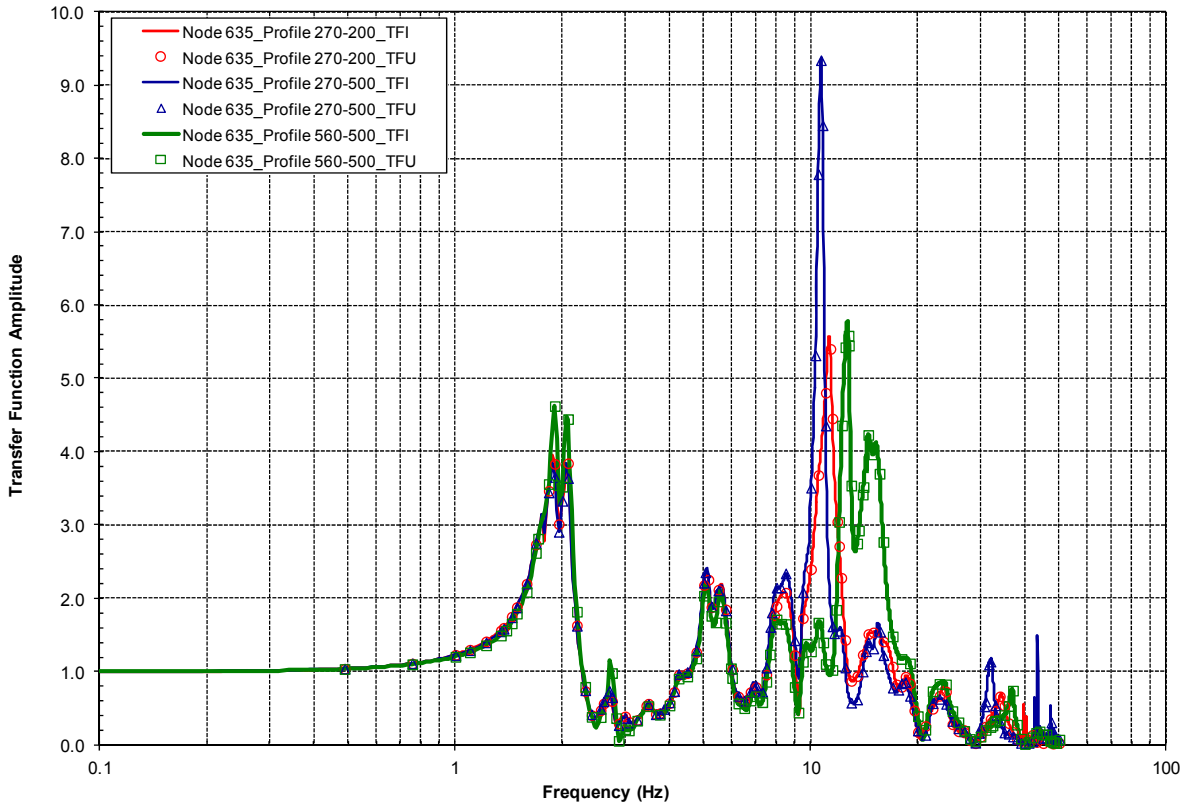

Figure A.2-5 Acceleration Transfer Functions for Subsurface Profiles 270-200, 270-500, and 560-500 for Y Direction (North-South) Due to Y Direction Ground Motion at Node 635

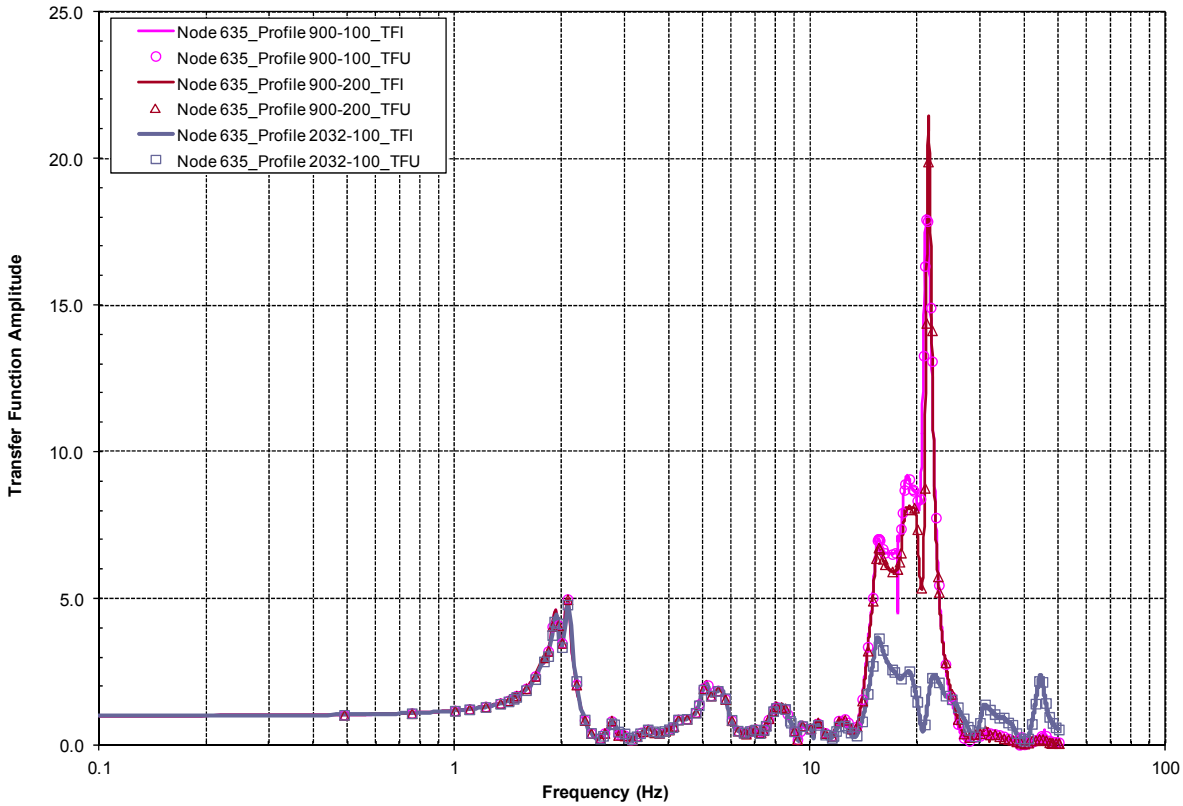

Figure A.2-6 Acceleration Transfer Functions for Subsurface Profiles 900-100 and 900-200, and 2032-100 for Y Direction (North-South) Due to Y Direction Ground Motion at Node 635

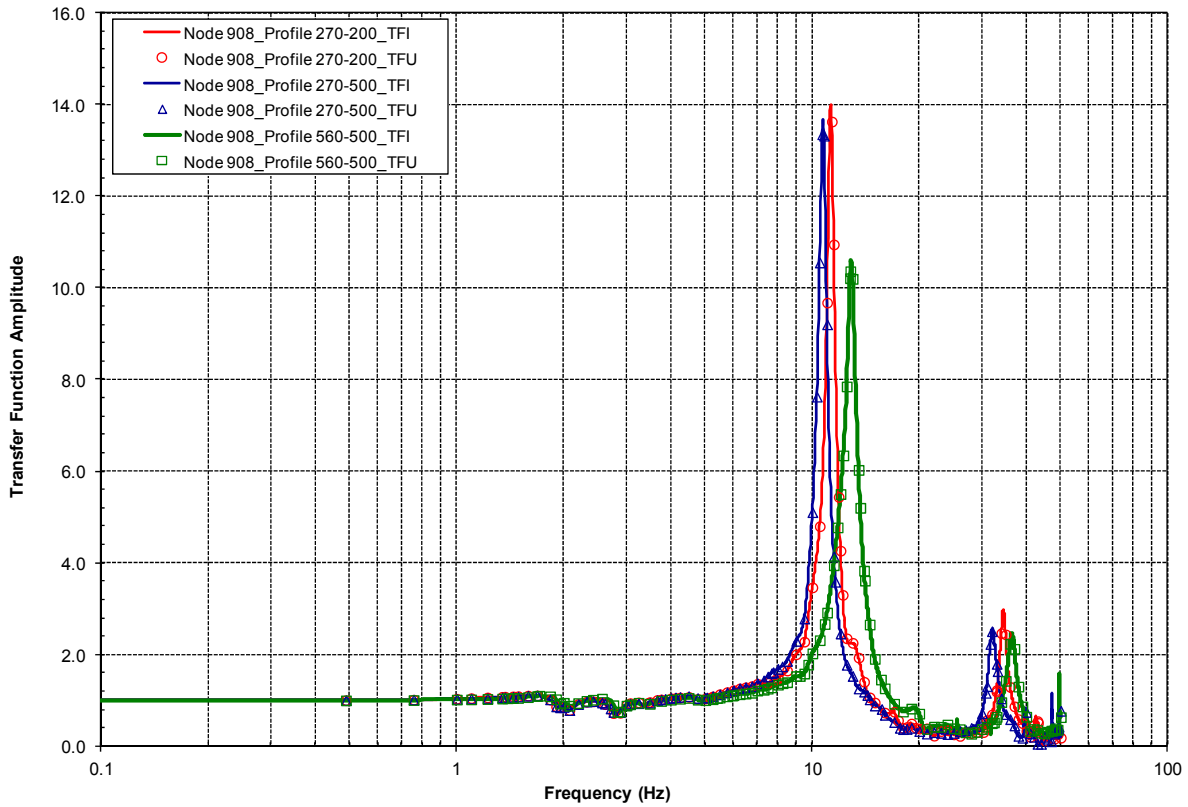

Figure A.2-7 Acceleration Transfer Functions for Subsurface Profiles 270-200, 270-500, and 560-500 for Y Direction (North-South) Due to Y Direction Ground Motion at Node 908

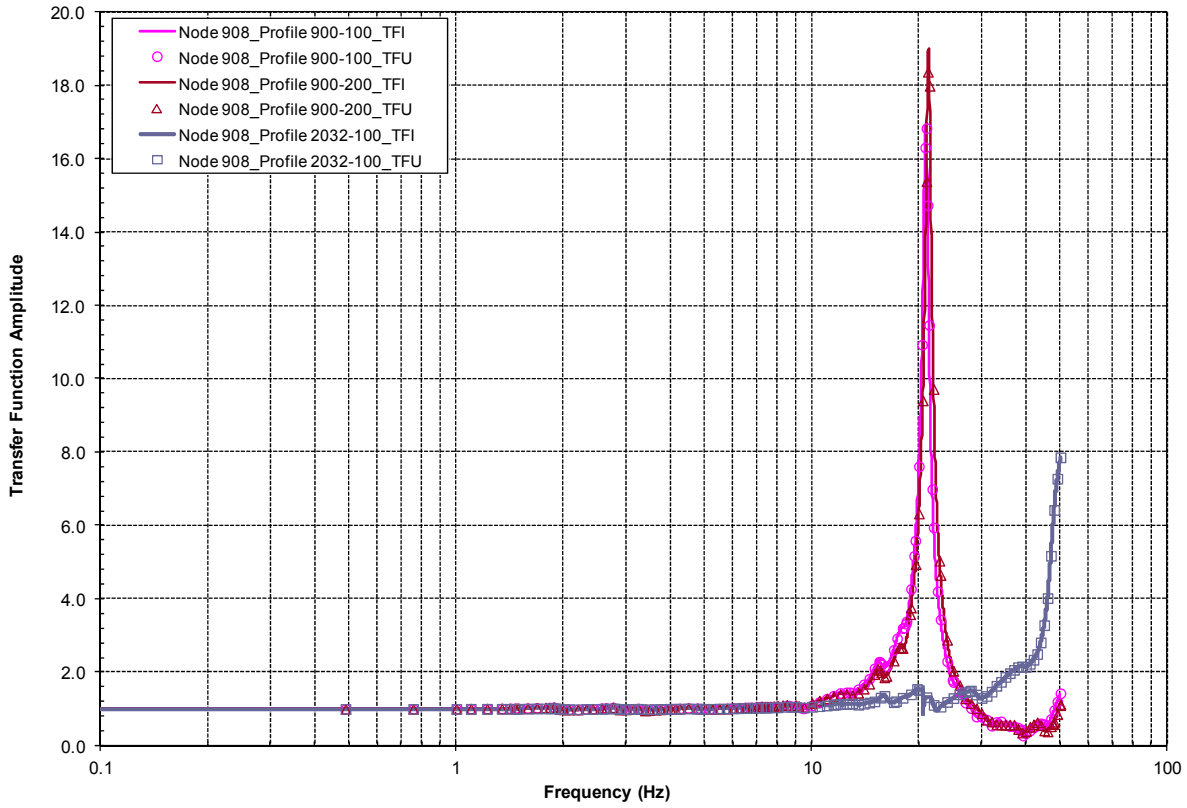

Figure A.2-8 Acceleration Transfer Functions for Subsurface Profiles 900-100 and 900-200, and 2032-100 for Y Direction (North-South) Due to Y Direction Ground Motion at Node 908

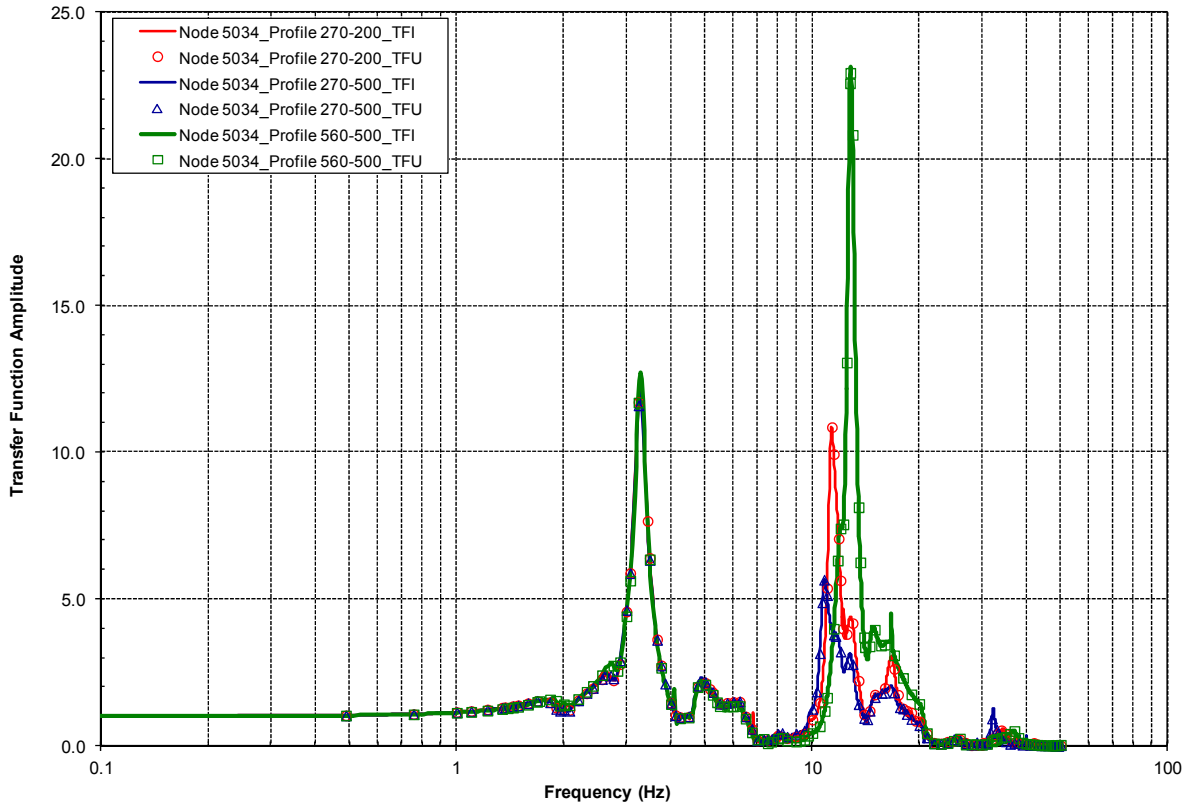

Figure A.2-9 Acceleration Transfer Functions for Subsurface Profiles 270-200, 270-500, and 560-500 for Y Direction (North-South) Due to Y Direction Ground Motion at Node 5034

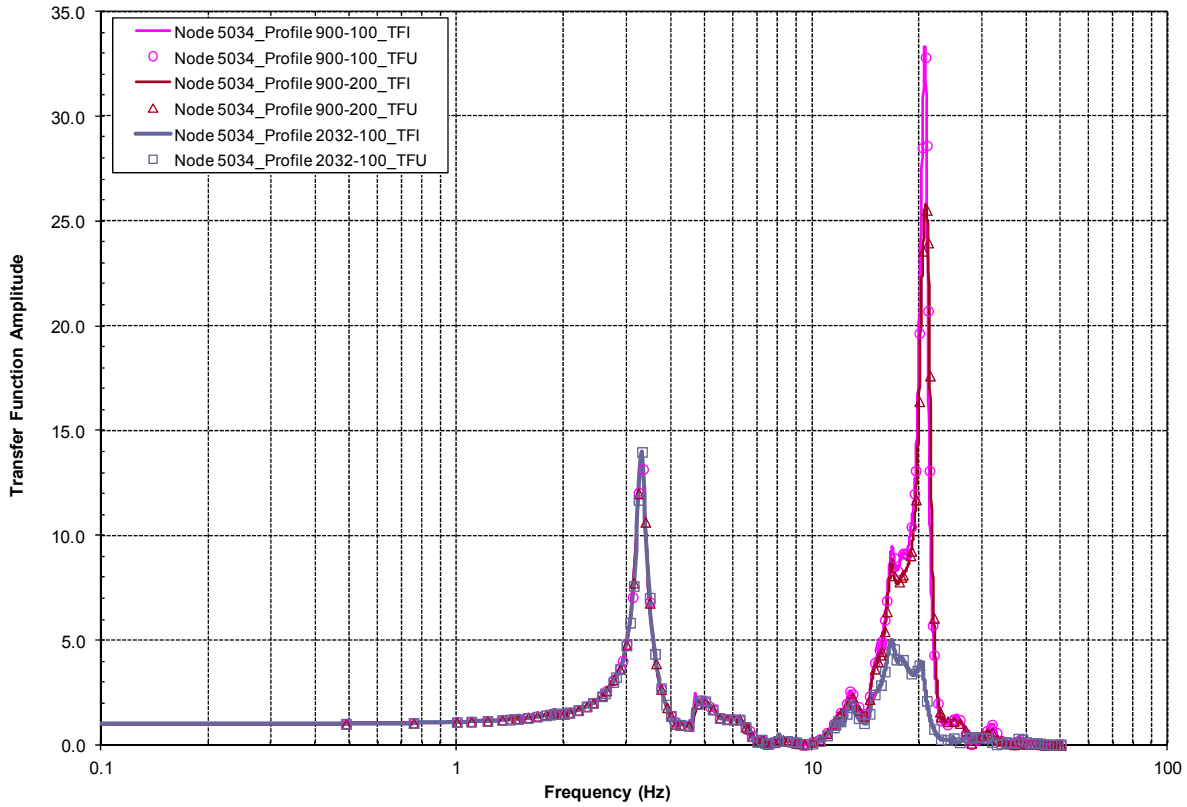

Figure A.2-10 Acceleration Transfer Functions for Subsurface Profiles 900-100 and 900-200, and 2032-100 for Y Direction (North-South) Due to Y Direction Ground Motion at Node 5034

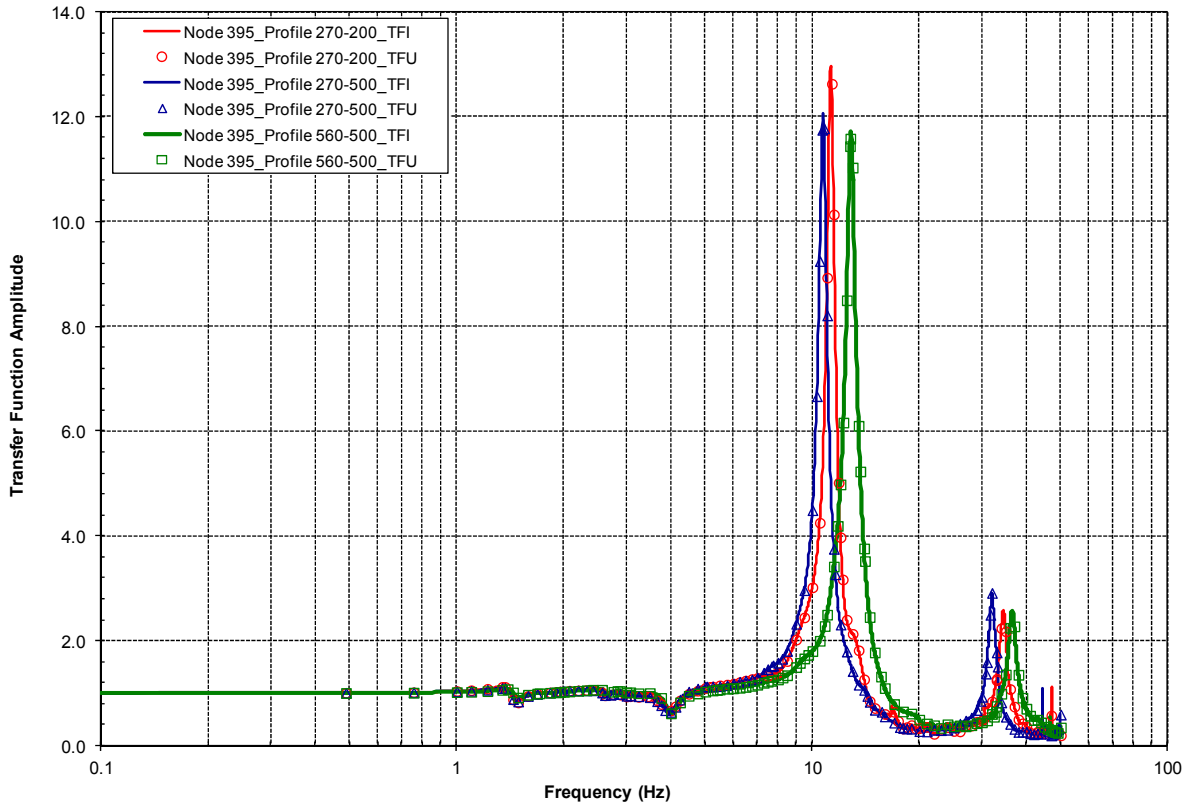

Figure A.2-11 Acceleration Transfer Functions for Subsurface Profiles 270-200, 270-500, and 560-500 for X Direction (East-West) Due to X Direction Ground Motion at Node 395

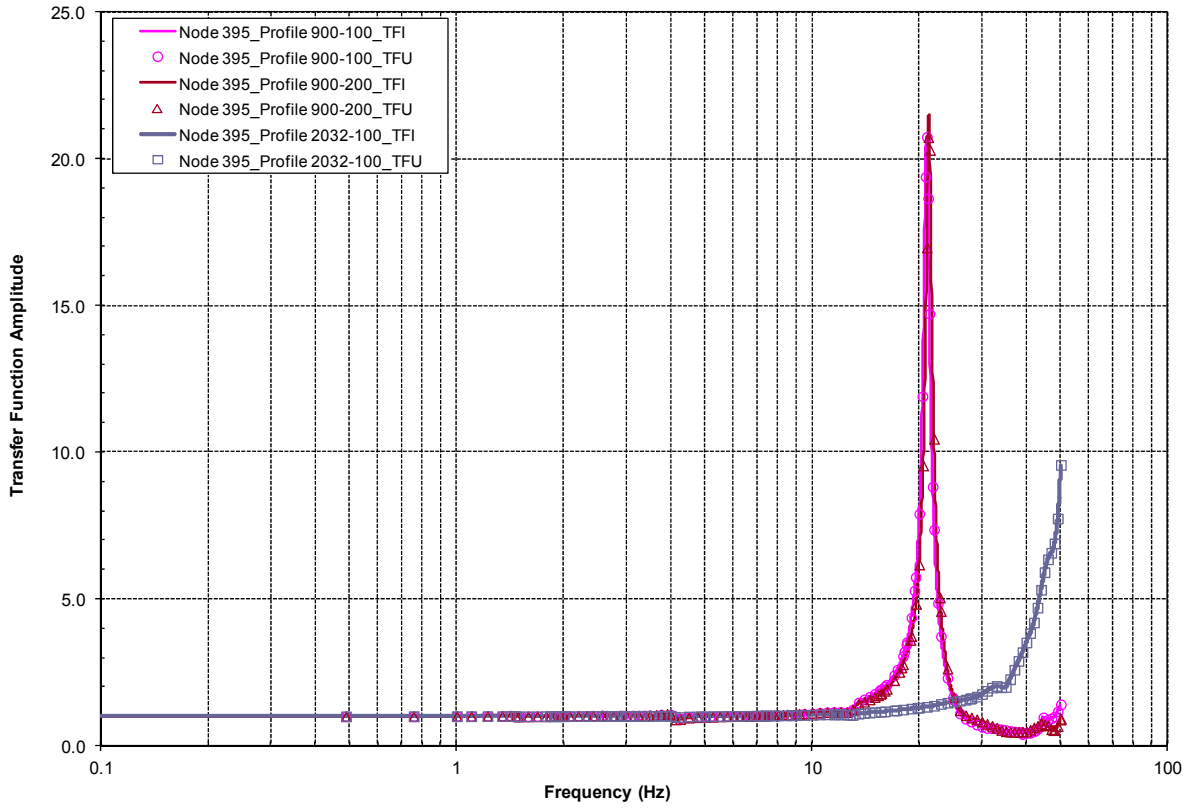

Figure A.2-12 Acceleration Transfer Functions for Subsurface Profiles 900-100 and 900-200, and 2032-100 for X Direction (East-West) Due to X Direction Ground Motion at Node 395

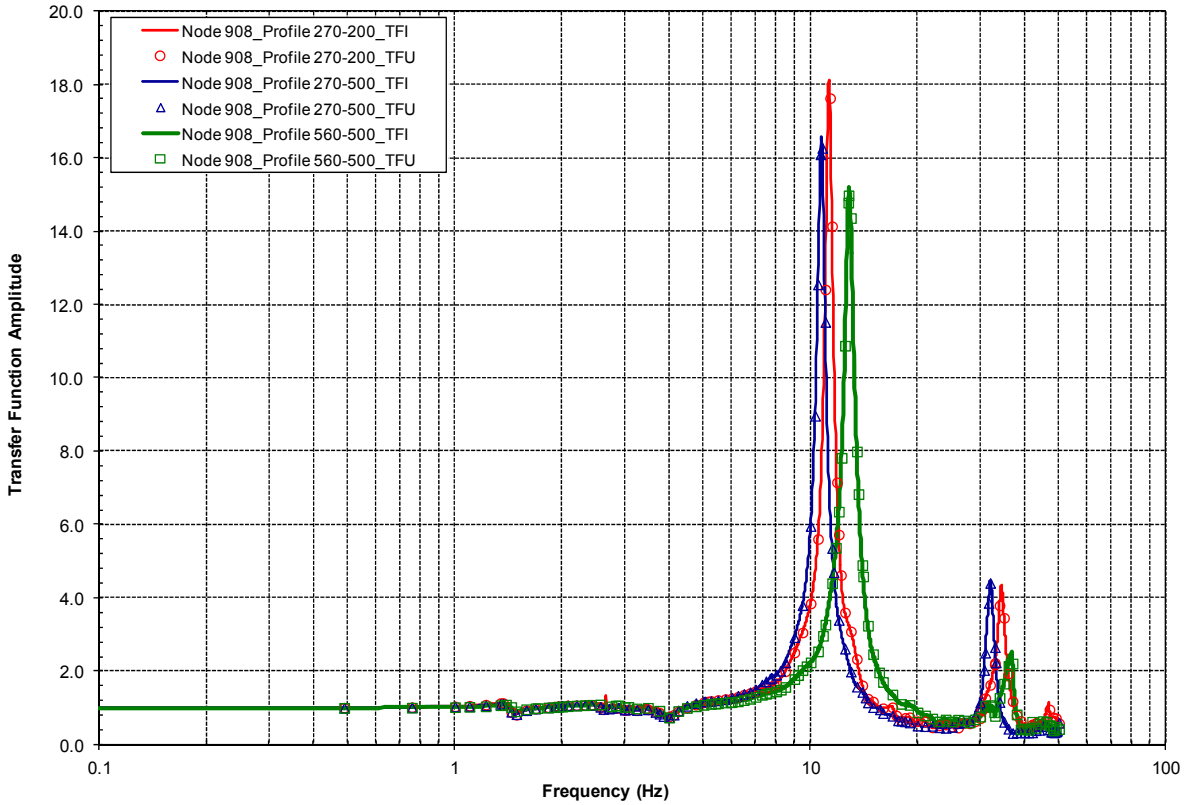

Figure A.2-13 Acceleration Transfer Functions for Subsurface Profiles 270-200, 270-500, and 560-500 for X Direction (East-West) Due to X Direction Ground Motion at Node 908

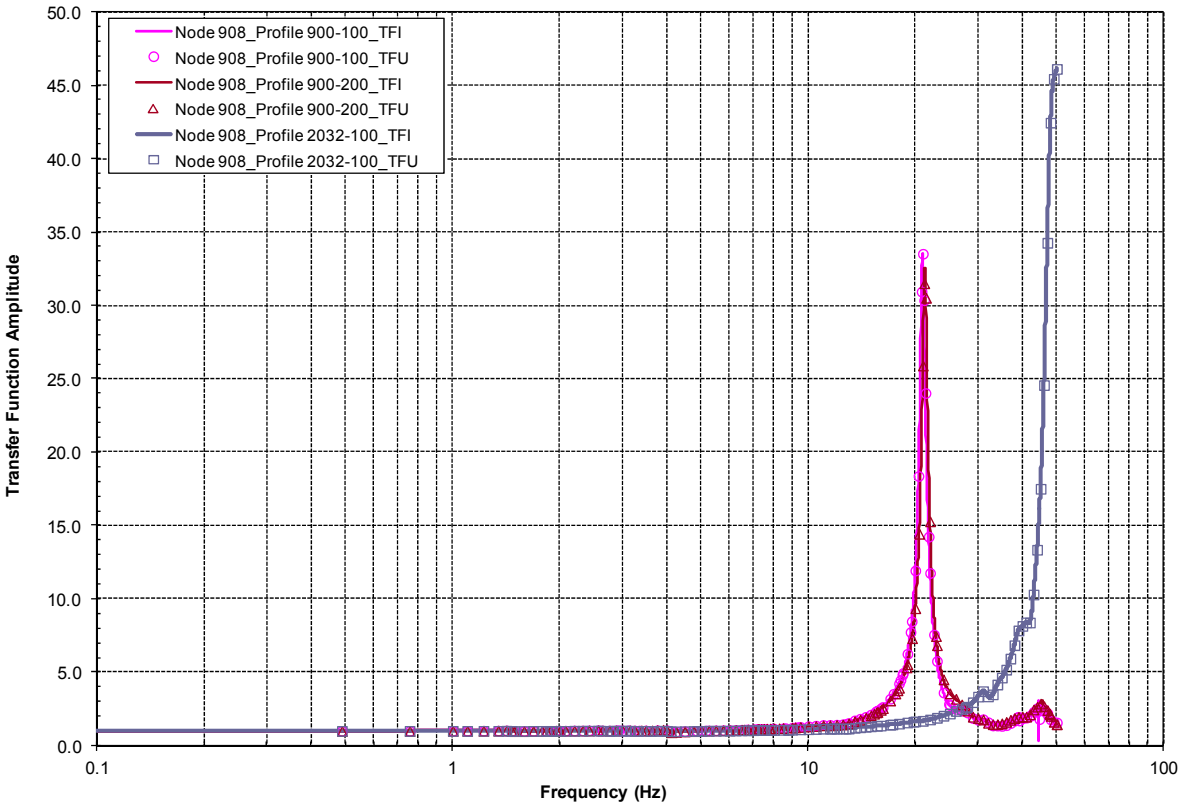

Figure A.2-14 Acceleration Transfer Functions for Subsurface Profiles 900-100 and 900-200, and 2032-100 for X Direction (East-West) Due to X Direction Ground Motion at Node 908

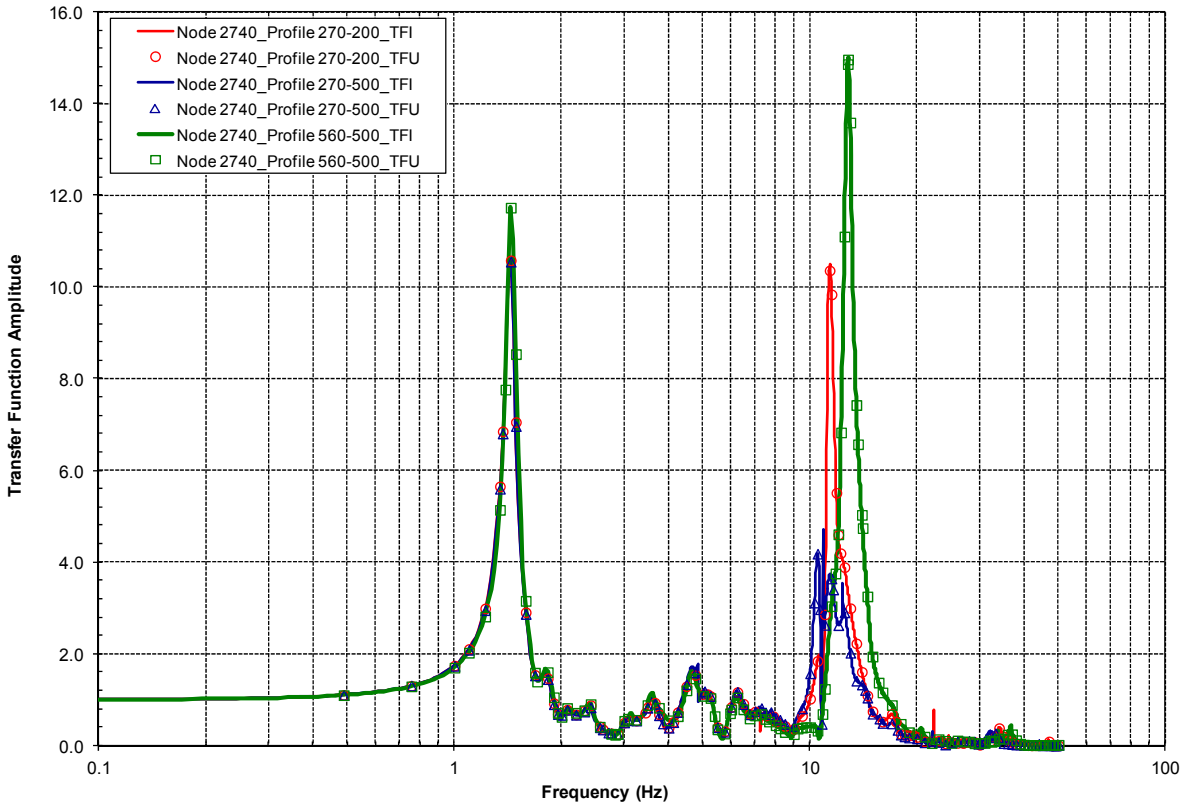

Figure A.2-15 Acceleration Transfer Functions for Subsurface Profiles 270-200, 270-500, and 560-500 for X Direction (East-West) Due to X Direction Ground Motion at Node 2740

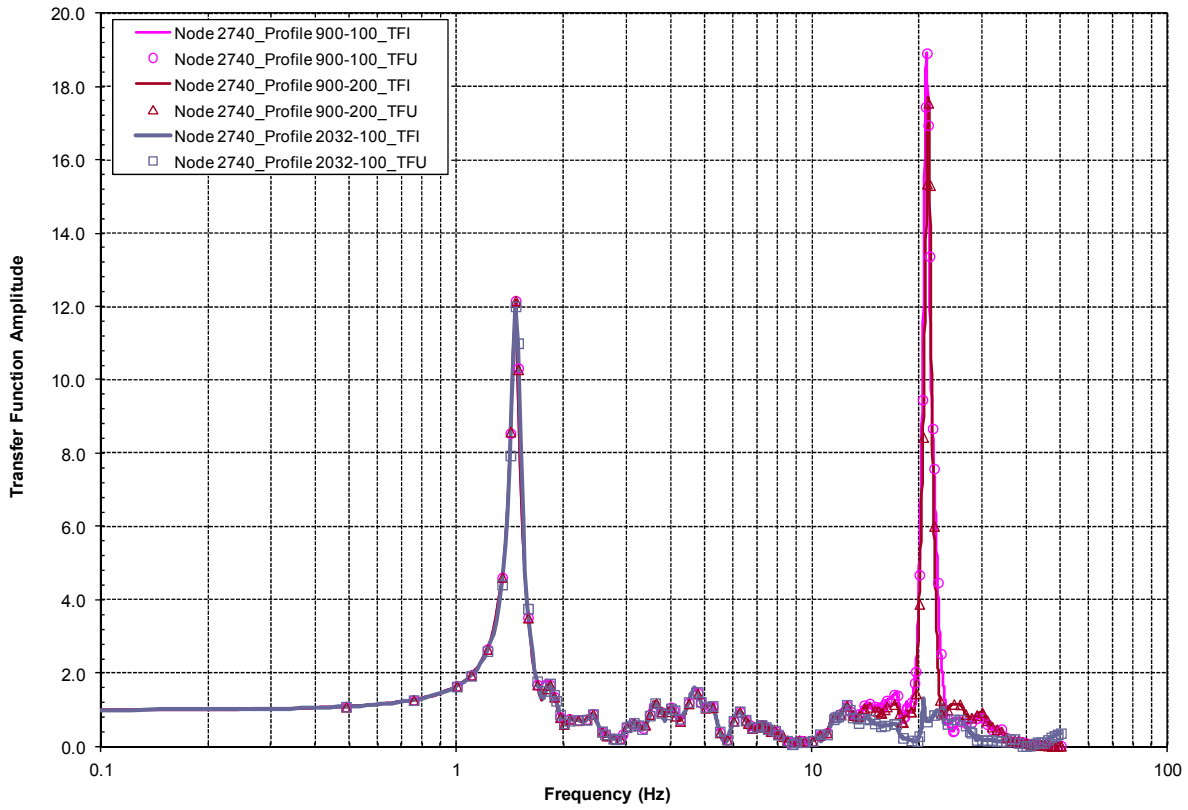

Figure A.2-16 Acceleration Transfer Functions for Subsurface Profiles 900-100 and 900-200, and 2032-100 for X Direction (East-West) Due to X Direction Ground Motion at Node 2740

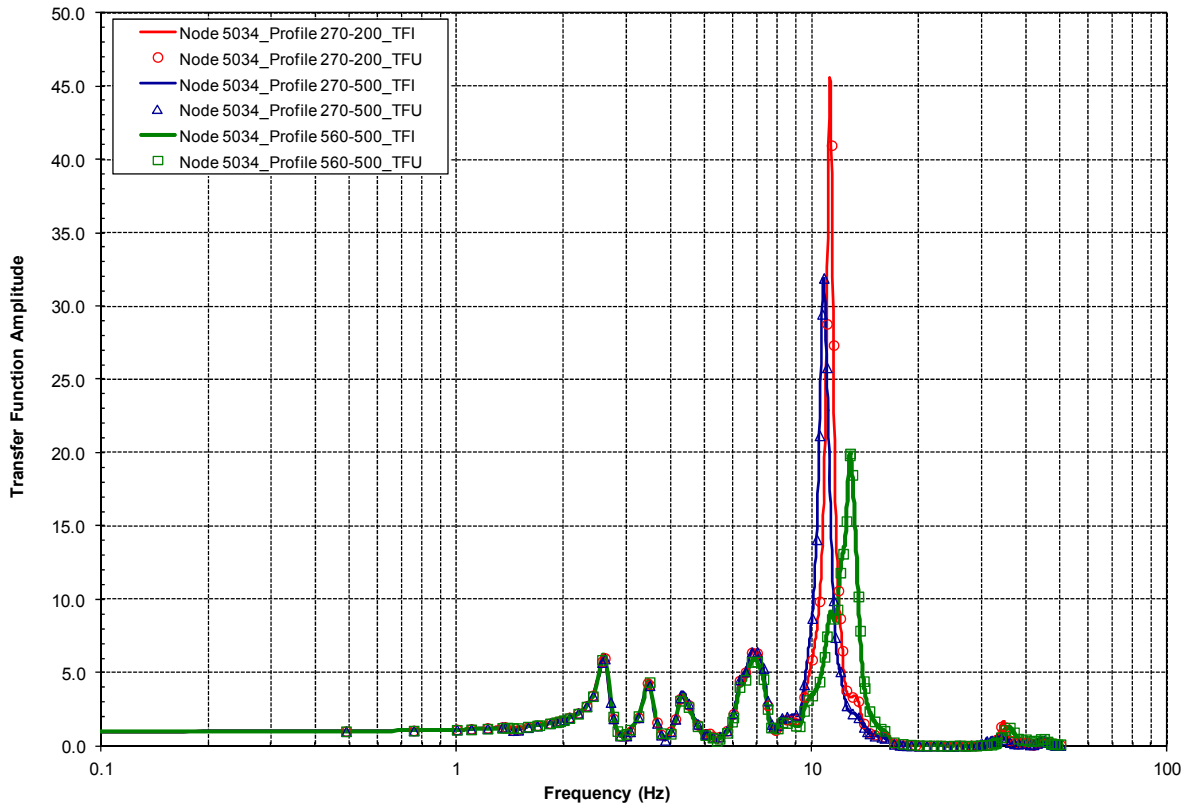

Figure A.2-17 Acceleration Transfer Functions for Subsurface Profiles 270-200, 270-500, and 560-500 for X Direction (East-West) Due to X Direction Ground Motion at Node 5034

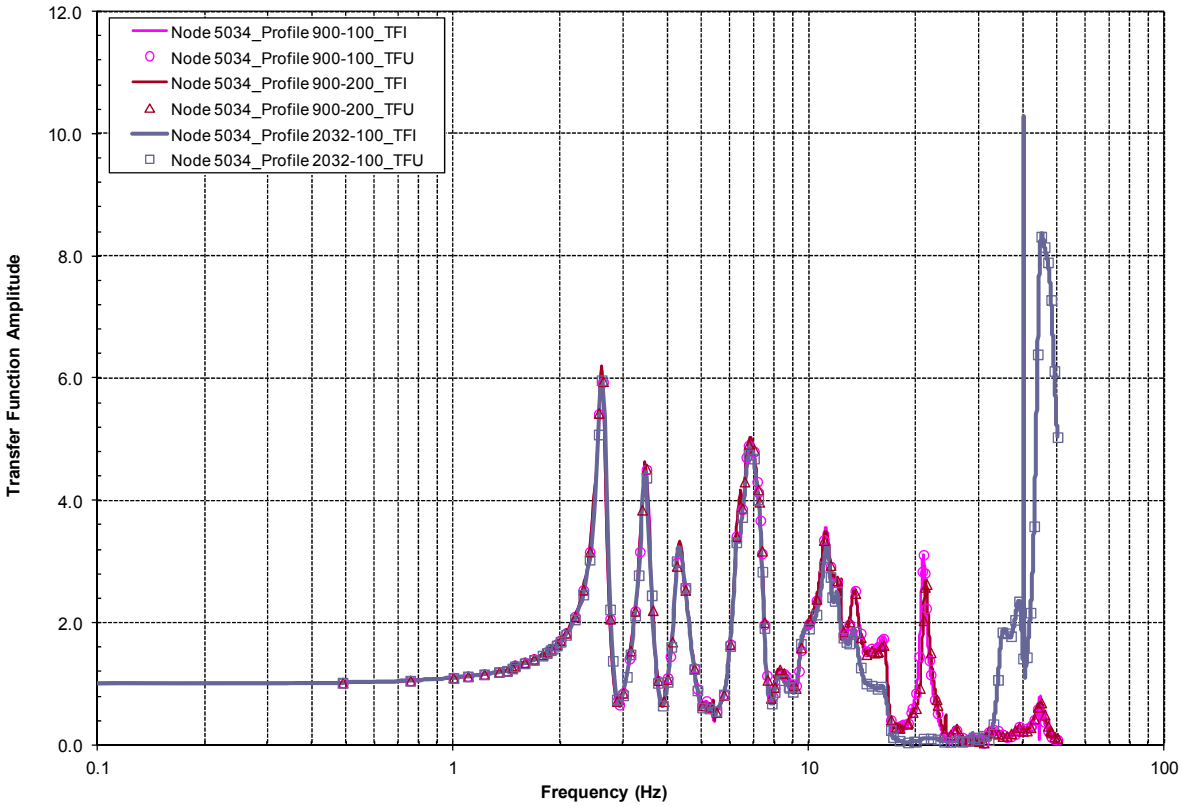

Figure A.2-18 Acceleration Transfer Functions for Subsurface Profiles 900-100 and 900-200, and 2032-100 for X Direction (East-West) Due to X Direction Ground Motion at Node 5034

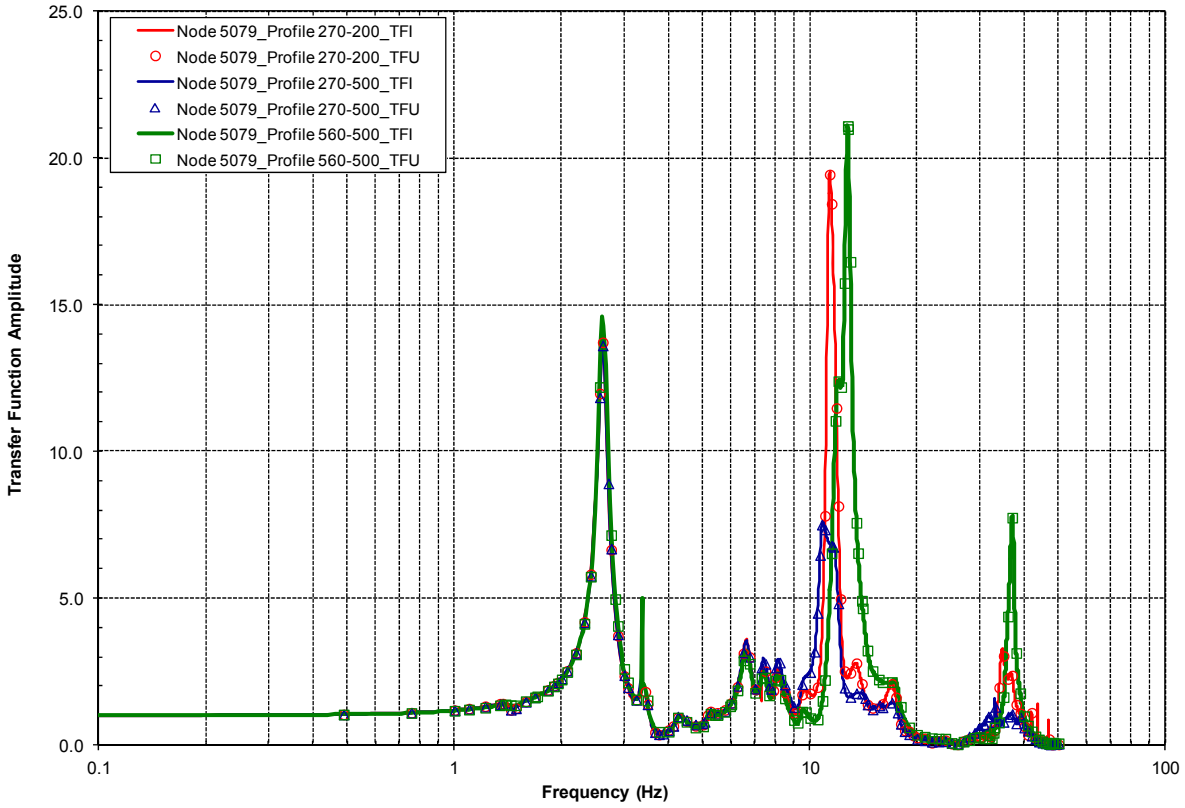

Figure A.2-19 Acceleration Transfer Functions for Subsurface Profiles 270-200, 270-500, and 560-500 for X Direction (East-West) Due to X Direction Ground Motion at Node 5079

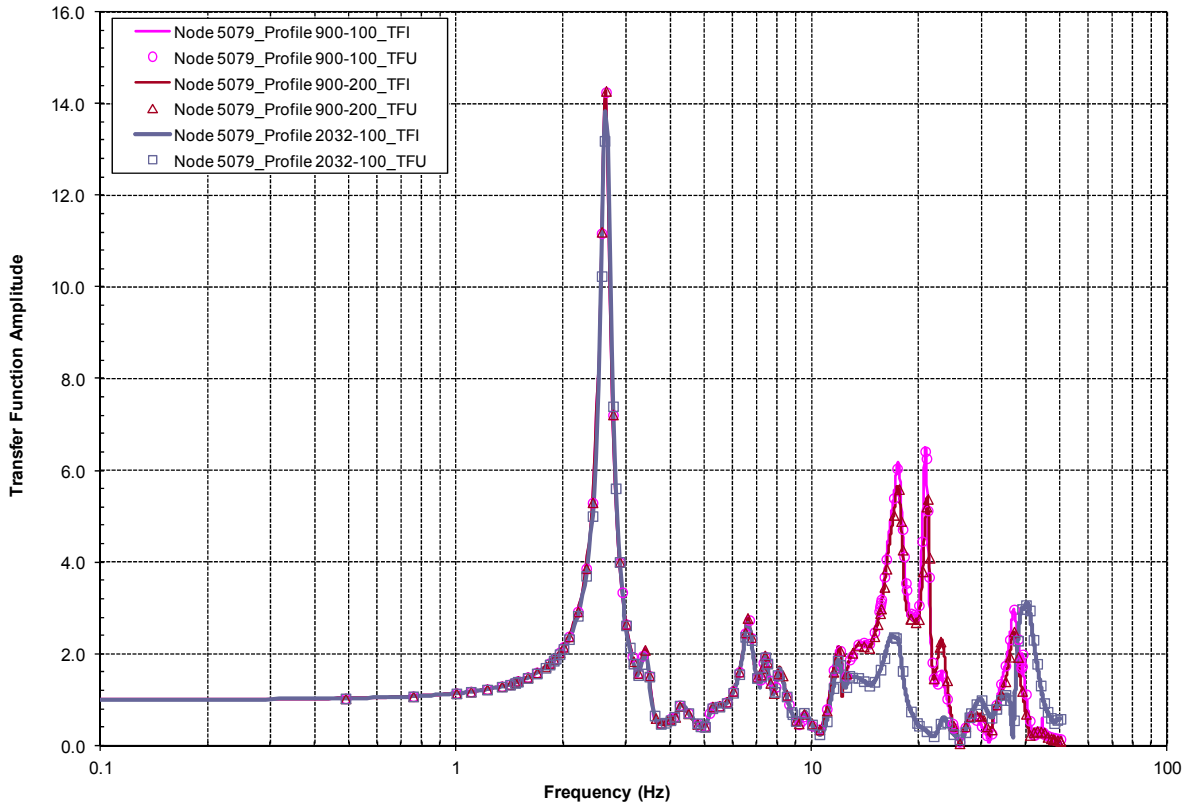

Figure A.2-20 Acceleration Transfer Functions for Subsurface Profiles 900-100 and 900-200, and 2032-100 for X Direction (East-West) Due to X Direction Ground Motion at Node 5079

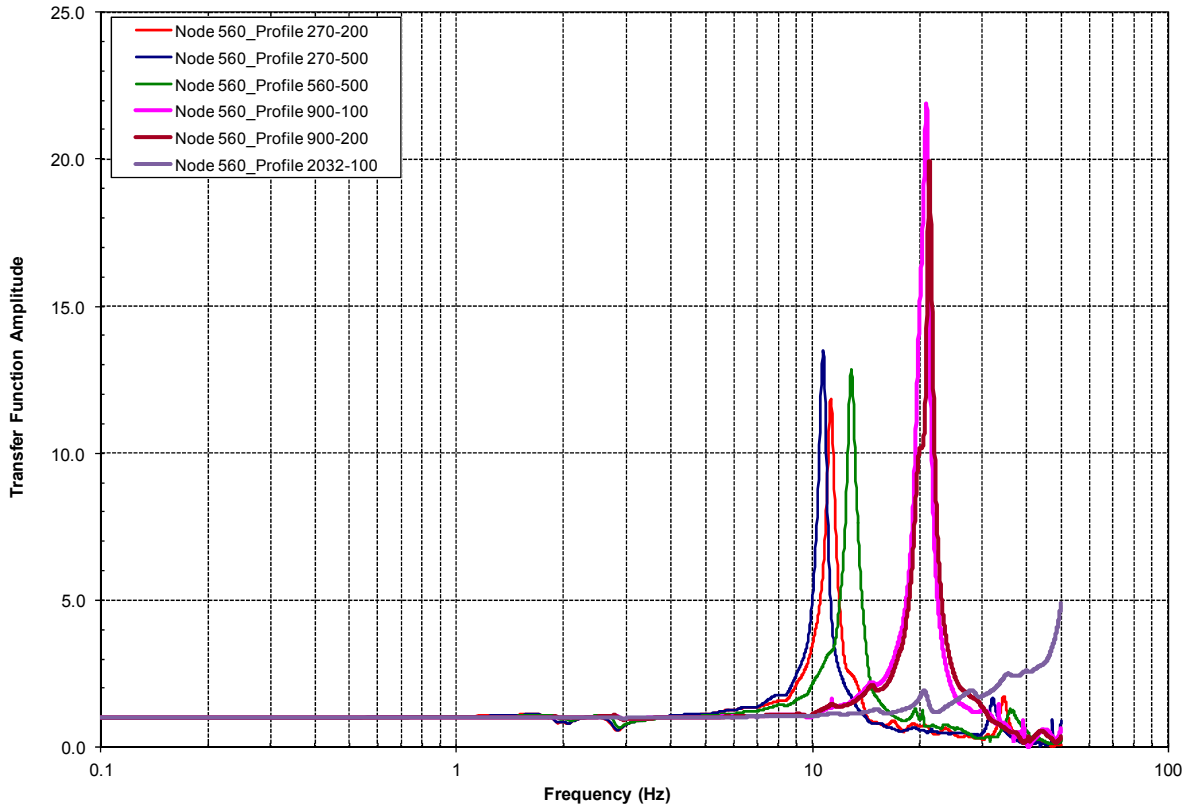

Figure A.2-21 Interpolated Acceleration Transfer Functions for all Six Subsurface Profiles for Y Direction (North-South) Due to Y Direction Ground Motion at Node 560

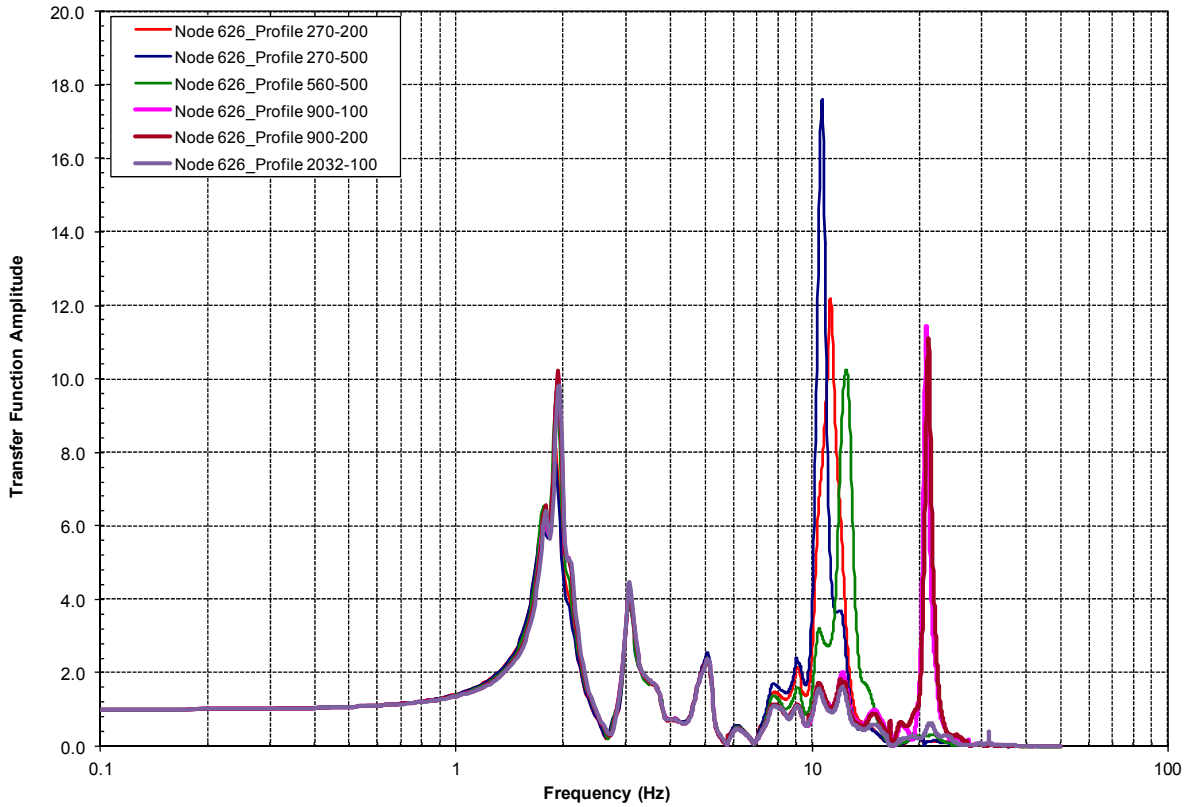

Figure A.2-22 Interpolated Acceleration Transfer Functions for all Six Subsurface Profiles for Y Direction (North-South) Due to Y Direction Ground Motion at Node 626

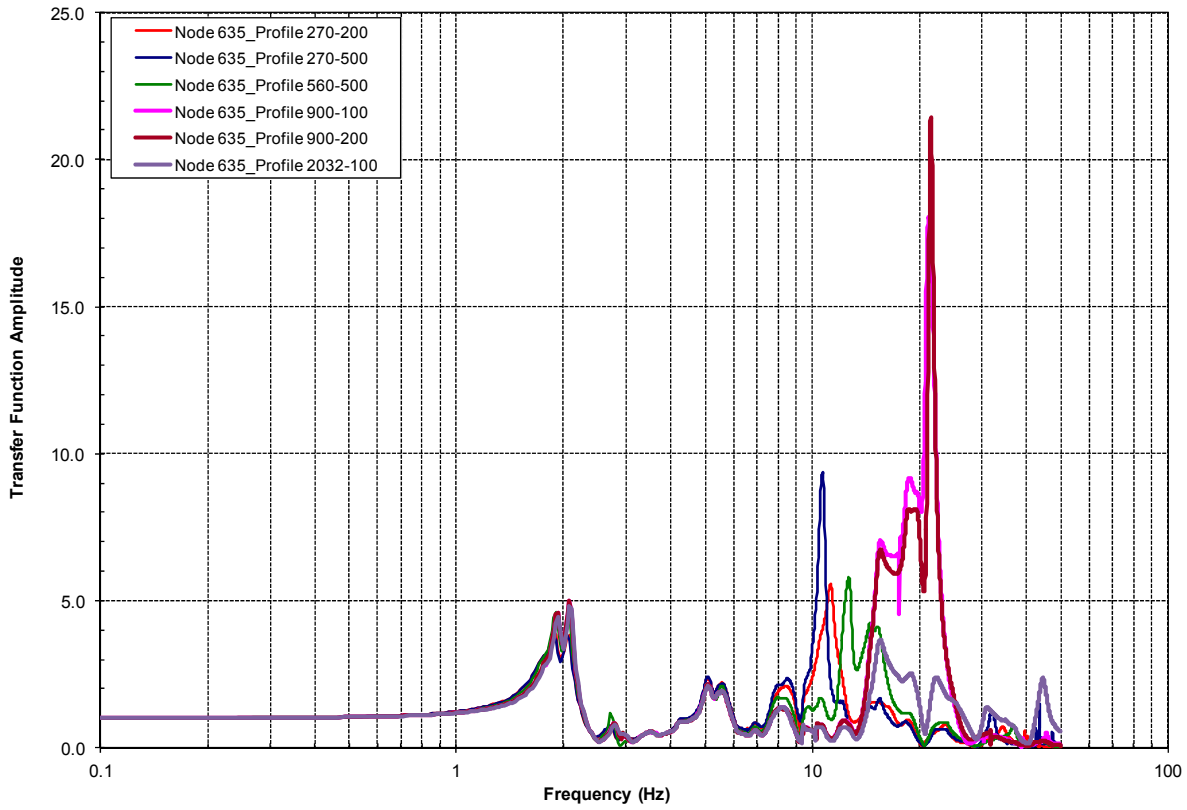

Figure A.2-23 Interpolated Acceleration Transfer Functions for all Six Subsurface Profiles for Y Direction (North-South) Due to Y Direction Ground Motion at Node 635

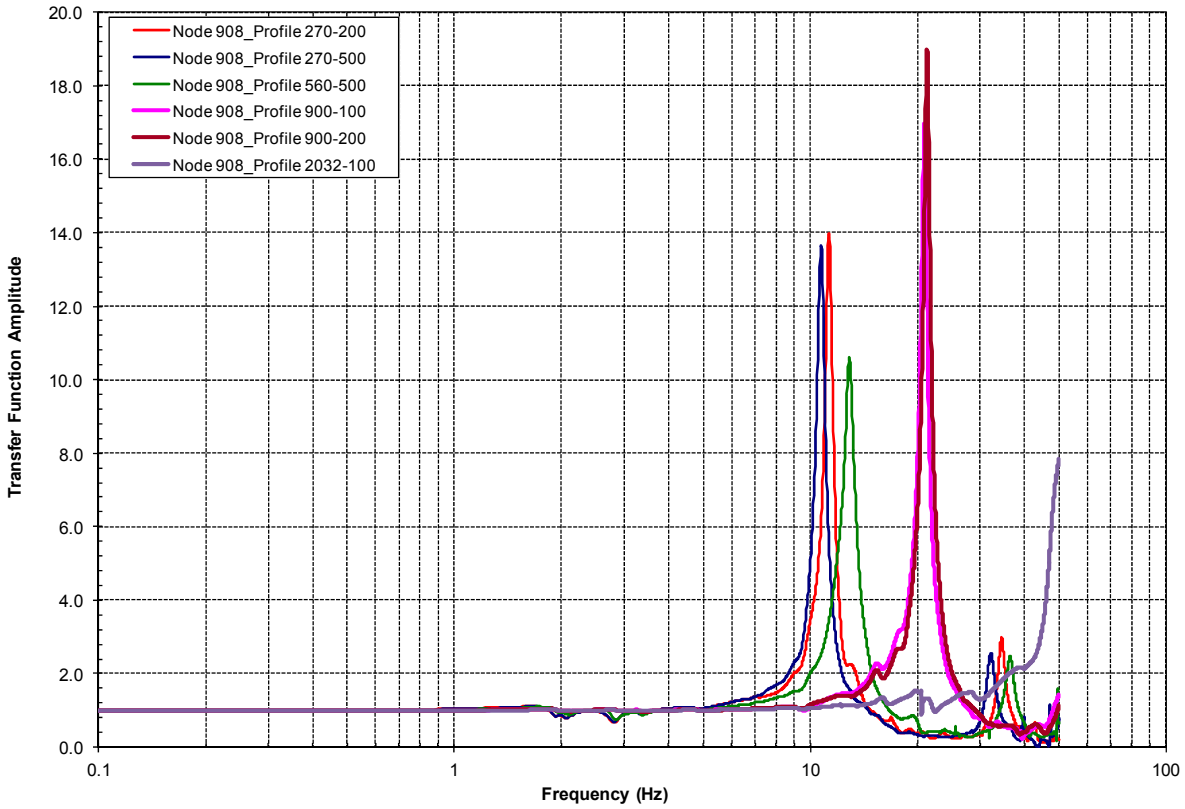

Figure A.2-24 Interpolated Acceleration Transfer Functions for all Six Subsurface Profiles for Y Direction (North-South) Due to Y Direction Ground Motion at Node 908

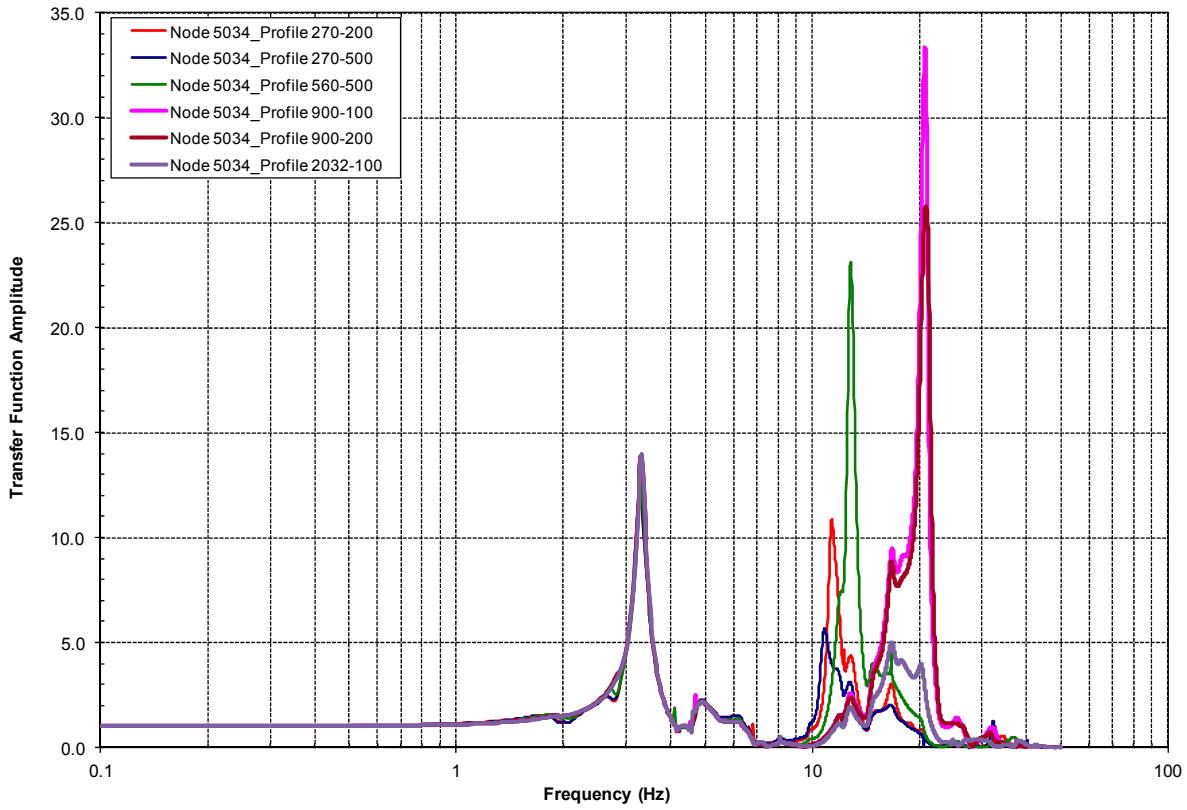

Figure A.2-25 Interpolated Acceleration Transfer Functions for all Six Subsurface Profiles for Y Direction (North-South) Due to Y Direction Ground Motion at Node 5034

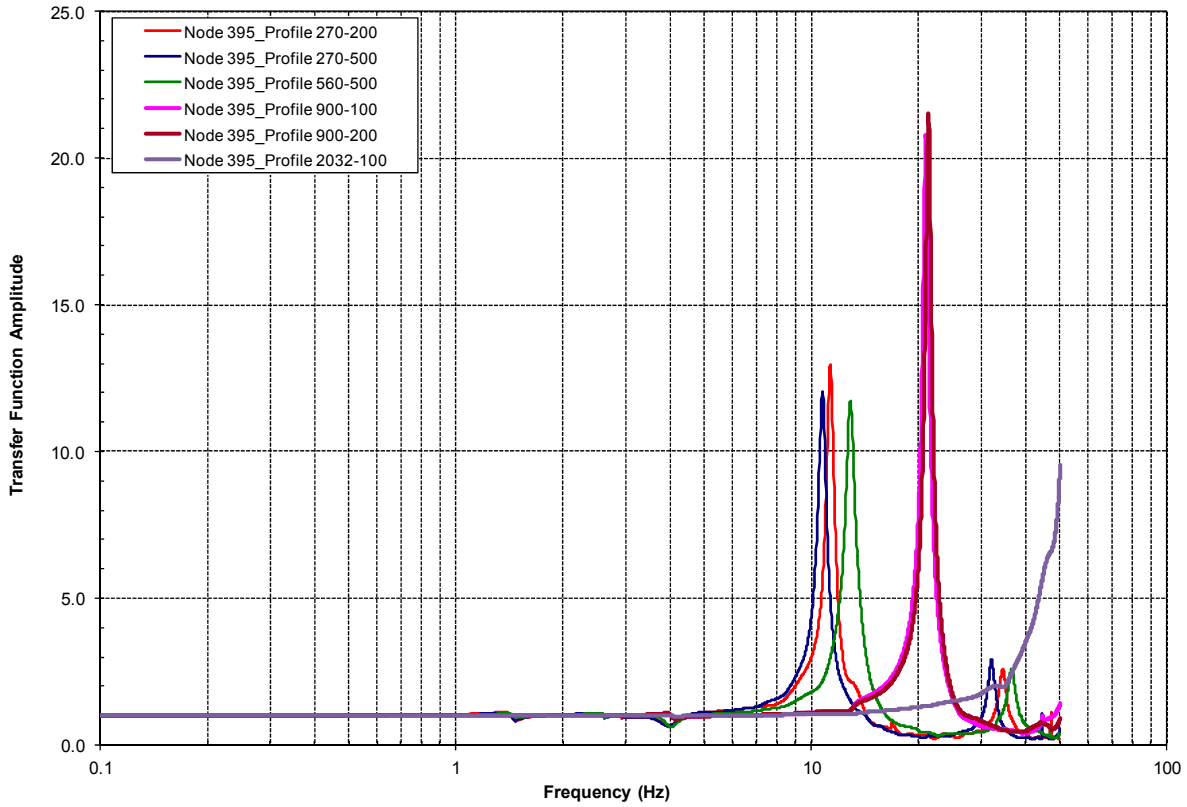

Figure A.2-26 Interpolated Acceleration Transfer Functions for all Six Subsurface Profiles for X Direction (East-West) Due to X Direction Ground Motion at Node 395

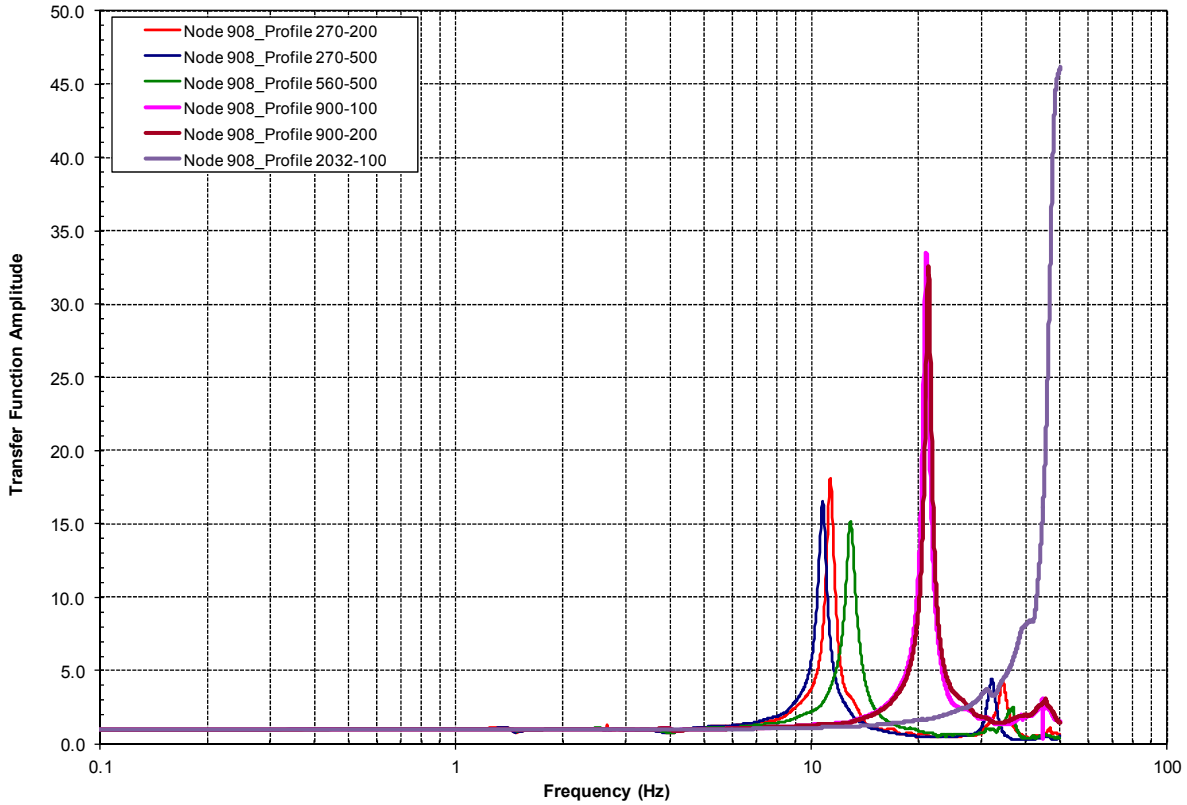

Figure A.2-27 Interpolated Acceleration Transfer Functions for all Six Subsurface Profiles for X Direction (East-West) Due to X Direction Ground Motion at Node 908

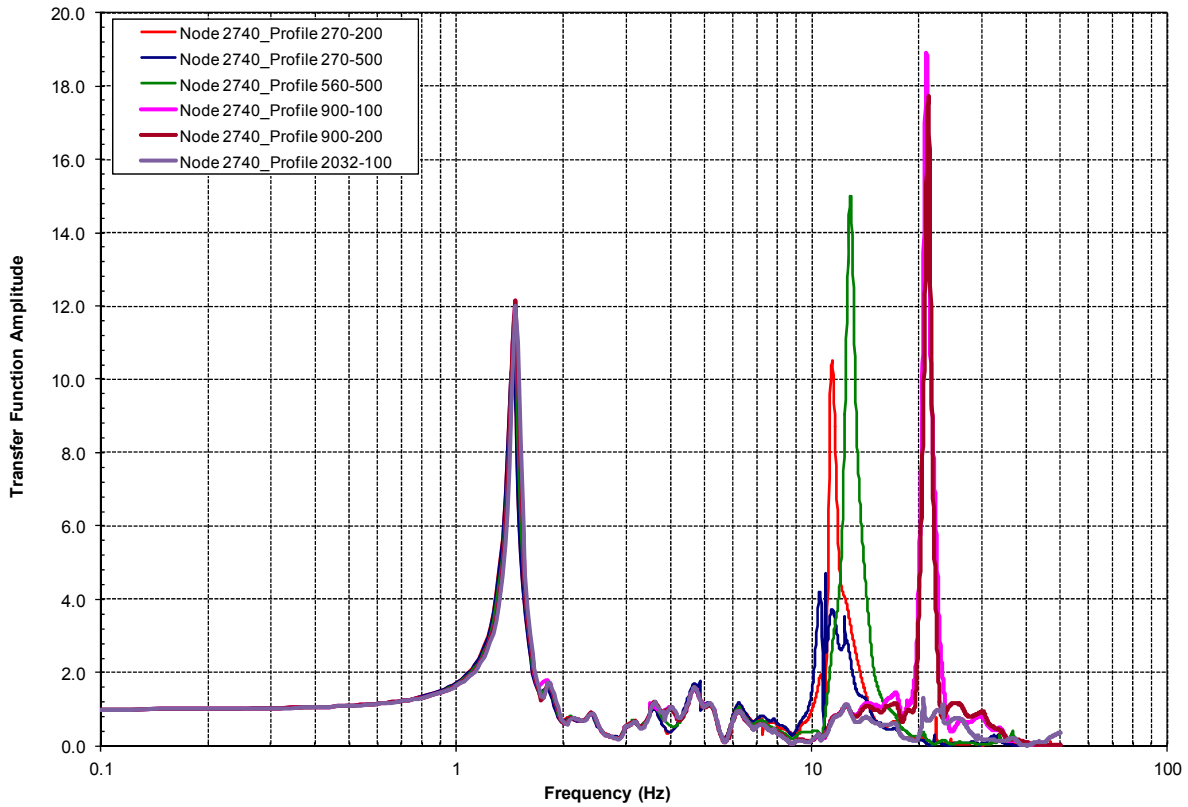

Figure A.2-28 Interpolated Acceleration Transfer Functions for all Six Subsurface Profiles for X Direction (East-West) Due to X Direction Ground Motion at Node 2740

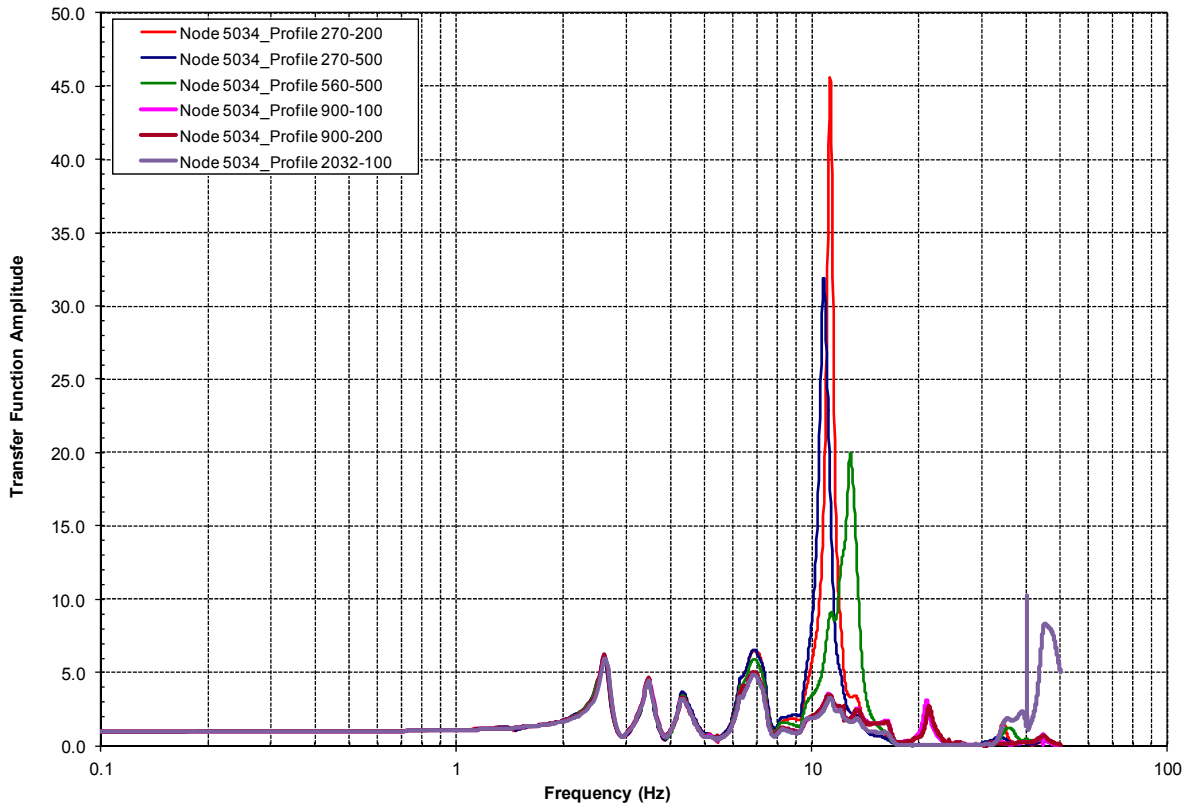

Figure A.2-29 Interpolated Acceleration Transfer Functions for all Six Subsurface Profiles for X Direction (East-West) Due to X Direction Ground Motion at Node 5034

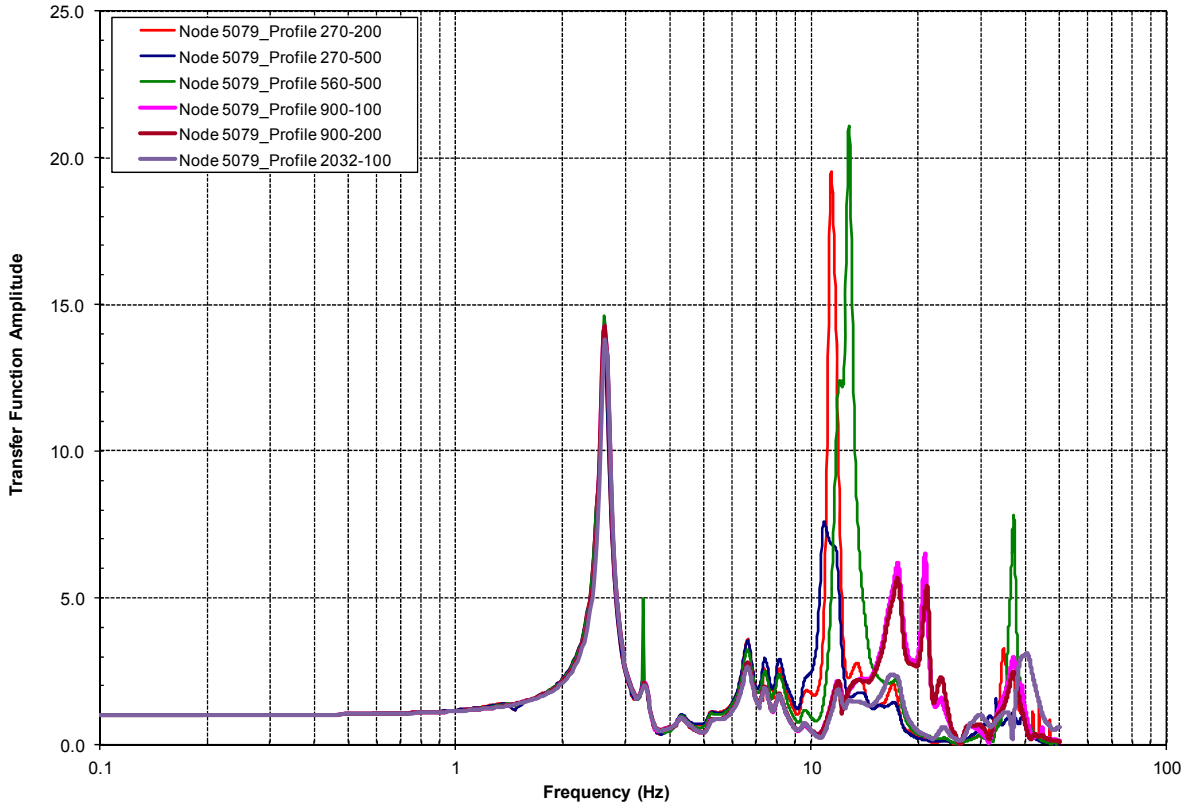

Figure A.2-30 Interpolated Acceleration Transfer Functions for all Six Subsurface Profiles for X Direction (East-West) Due to X Direction Ground Motion at Node 5079

A.3.0 RESULTS OF MAXIMUM T/B COMPLEX DISPLACEMENTS

Tables A.3-1 and A.3-2 report the SSI computed maximum relative T/B complex displacements in the X (East-West) and Y (North-South) directions at the 66 T/B and Electrical Room nodes with respect to the free-field input ground surface motion for the six subsurface profiles.

For the selected nodes adjacent to the R/B complex (Figure 4.3-1), the maximum displacements in the Y-direction (North-South) range from 0.0760 inch at node 290 to 2.3784 inches at node 605 (Table A.3-2). For each of the 66 selected nodes, Table A.3-3 shows the subsurface profile associated with the computed maximum relative X and Y direction displacements with respect to free-field motion.

Table A.3-1 Maximum Relative Displacement in X Direction (East-West) Relative to Free-Field Input Motion (Uncracked Case)

(Sheet 1 of 2)

Node No.	Elevation (feet)	X-Direction (East-West) Displacement (inch)						
		Subsurface Profile						Enveloping Maximum
		270-200	270-500	560-500	900-100	900-200	2032-100	
290	2.75	0.1343	0.1314	0.0941	0.0222	0.0237	0.0051	0.1343
338	2.75	0.1529	0.1497	0.1038	0.0273	0.0291	0.0111	0.1529
386	2.75	0.1589	0.1524	0.1037	0.0280	0.0298	0.0139	0.1589
389	2.75	0.1609	0.1578	0.1032	0.0276	0.0297	0.0134	0.1609
392	2.75	0.1456	0.1401	0.0887	0.0184	0.0209	0.0078	0.1456
395	2.75	0.1336	0.1281	0.0777	0.0135	0.0158	0.0055	0.1336
398	2.75	0.1272	0.1224	0.0711	0.0132	0.0155	0.0053	0.1272
401	2.75	0.1218	0.1159	0.0705	0.0137	0.0161	0.0061	0.1218
473	2.75	0.1599	0.1549	0.1037	0.0280	0.0295	0.0147	0.1599
560	2.75	0.1595	0.1534	0.1038	0.0304	0.0317	0.0153	0.1595
676	2.75	0.1541	0.1482	0.1021	0.0329	0.0347	0.0155	0.1541
792	2.75	0.1393	0.1346	0.0962	0.0328	0.0344	0.0133	0.1393
879	2.75	0.1126	0.1094	0.0818	0.0254	0.0265	0.0056	0.1126
908	2.75	0.1495	0.1530	0.1044	0.0284	0.0302	0.0135	0.1530
911	2.75	0.1598	0.1569	0.1031	0.0276	0.0298	0.0138	0.1598
914	2.75	0.1441	0.1379	0.0877	0.0181	0.0204	0.0076	0.1441
917	2.75	0.1326	0.1271	0.0772	0.0130	0.0152	0.0050	0.1326
920	2.75	0.1266	0.1219	0.0717	0.0130	0.0154	0.0054	0.1266
923	2.75	0.1201	0.1146	0.0689	0.0124	0.0148	0.0049	0.1201
544	24.75	1.3891	1.3728	1.5253	1.5306	1.5269	1.4885	1.5306
606	24.75	1.4102	1.3953	1.5530	1.5616	1.5566	1.5175	1.5616
627	24.75	1.4302	1.4188	1.5812	1.5963	1.5885	1.5481	1.5963
630	24.75	1.4443	1.4448	1.5997	1.6201	1.6101	1.5666	1.6201
633	24.75	1.4406	1.4447	1.5976	1.6190	1.6090	1.5589	1.6190
636	24.75	1.4290	1.4296	1.5838	1.6047	1.5945	1.5930	1.6047
4965	24.75	0.8495	0.8674	0.9031	0.8980	0.9141	0.8939	0.9141
4968	24.75	0.8540	0.8720	0.9066	0.9027	0.9196	0.8988	0.9196
5035	24.75	0.8445	0.8621	0.8962	0.8919	0.9080	0.8879	0.9080
570	33.5	0.7746	0.7549	0.7507	0.6970	0.7016	0.6584	0.7746
753	33.5	1.5464	1.5235	1.6207	1.5637	1.5680	1.4901	1.6207
1411	33.5	1.3552	1.3515	1.3925	1.3252	1.3283	1.2611	1.3925
2657	33.5	1.4789	1.4596	1.4611	1.4001	1.4043	1.3377	1.4789
2738	33.5	1.9632	1.9429	1.9752	1.8507	1.8734	1.7943	1.9752

Table A.3-1 Maximum Relative Displacement in X Direction (East-West) Relative to Free-Field Input Motion (Uncracked Case)

(Sheet 2 of 2)

Node No.	Elevation (feet)	X-Direction (East-West) Displacement (inch)						
		Subsurface Profile						Enveloping Maximum
		270-200	270-500	560-500	900-100	900-200	2032-100	
5039	33.5	0.7220	0.7323	0.6980	0.6277	0.6283	0.6091	0.7323
5042	33.5	1.7028	1.7400	1.7589	1.7484	1.7369	1.6998	1.7589
5045	33.5	2.3197	2.3544	2.4252	2.4546	2.4694	2.4079	2.4694
5048	33.5	1.7510	1.7687	1.8364	1.8347	1.8509	1.7993	1.8509
5080	33.5	0.9604	0.9757	0.9512	0.9379	0.9454	0.9104	0.9757
542	60.5	2.0983	2.0486	2.1457	2.1298	2.1474	2.0205	2.1474
573	60.5	1.5263	1.4984	1.5235	1.4624	1.4683	1.3940	1.5263
605	60.5	2.0872	2.0362	2.1369	2.1218	2.1413	2.0200	2.1413
626	60.5	2.1208	2.0509	2.1865	2.1640	2.1799	2.0790	2.1865
629	60.5	2.1641	2.1145	2.2558	2.2365	2.2500	2.1694	2.2558
632	60.5	2.1852	2.1412	2.2850	2.2687	2.2728	2.2123	2.2850
635	60.5	2.2161	2.1761	2.3208	2.3058	2.3102	2.2308	2.3208
755	60.5	3.1443	3.1809	3.4236	3.2656	3.3112	3.1188	3.4236
1421	60.5	2.8771	2.8775	2.9631	2.8138	2.8349	2.6917	2.9631
2659	60.5	2.7952	2.7871	2.7957	2.6532	2.6358	2.8175	2.8175
2740	60.5	2.7273	2.7079	2.7444	2.5765	2.6097	2.5734	2.7444
4964	63.5	0.8417	0.8349	0.8370	0.8175	0.8260	0.8077	0.8417
4967	63.5	0.8398	0.8329	0.8333	0.8137	0.8224	0.8041	0.8398
5034	63.5	0.8433	0.8362	0.8365	0.8166	0.8257	0.8071	0.8433
5037	63.5	0.8958	0.9147	0.9106	0.8880	0.8953	0.8672	0.9147
5041	63.5	1.7226	1.7727	1.8407	1.8459	1.8580	1.8007	1.8580
5044	63.5	2.3804	2.4234	2.5313	2.5592	2.5672	2.5085	2.5672
5047	63.5	2.1547	2.1955	2.2656	2.2680	2.2774	2.2212	2.2774
5079	63.5	1.6161	1.6580	1.6543	1.6645	1.6654	1.6217	1.6654
574	87.6667	2.3204	2.2881	2.3303	2.2482	2.2575	2.1629	2.3303
756	87.6667	4.8713	4.8518	4.9982	4.6741	4.6904	4.6290	4.9982
1422	87.6667	5.2350	5.2331	5.2860	4.9685	4.9584	5.2774	5.2860
2660	87.6667	5.0978	5.0765	5.0576	4.7429	4.7186	5.0502	5.0978
2741	87.6667	3.9321	3.9086	3.9846	3.7891	3.8338	4.0293	4.0293
661	169.417	3.6783	3.6628	3.7260	3.6692	3.6759	3.6589	3.7260
745	169.417	3.7358	3.7177	3.8110	3.7880	3.7986	3.7153	3.8110
3164	169.417	3.4896	3.4871	3.8095	3.9370	3.9484	3.9183	3.9484
3210	169.417	3.5457	3.5405	3.8405	3.9798	4.0050	3.9691	4.0050

Table A.3-2 Maximum Relative Displacement in Y Direction (North-South) Relative to Free-Field Input Motion (Uncracked Case)

(Sheet 1 of 2)

Node No.	Elevation (feet)	Maximum Nodal Displacements (inch)						
		Subsurface Profile						Enveloping Maximum
		270-200	270-500	560-500	900-100	900-200	2032-100	
290	2.75	0.0756	0.0760	0.0528	0.0117	0.0123	0.0033	0.0760
338	2.75	0.0965	0.0932	0.0588	0.0189	0.0197	0.0109	0.0965
386	2.75	0.1095	0.1068	0.0732	0.0223	0.0234	0.0102	0.1095
389	2.75	0.1102	0.1088	0.0780	0.0284	0.0301	0.0123	0.1102
392	2.75	0.1009	0.0980	0.0669	0.0203	0.0222	0.0108	0.1009
395	2.75	0.1002	0.1006	0.0685	0.0216	0.0234	0.0143	0.1006
398	2.75	0.1049	0.1073	0.0762	0.0297	0.0316	0.0221	0.1073
401	2.75	0.1080	0.1121	0.0785	0.0320	0.0337	0.0246	0.1121
473	2.75	0.1086	0.1060	0.0719	0.0232	0.0247	0.0116	0.1086
560	2.75	0.1088	0.1114	0.0739	0.0225	0.0235	0.0103	0.1114
676	2.75	0.1212	0.1258	0.0856	0.0236	0.0255	0.0110	0.1258
792	2.75	0.1268	0.1316	0.0938	0.0298	0.0310	0.0137	0.1316
879	2.75	0.1047	0.1108	0.0779	0.0220	0.0232	0.0049	0.1108
908	2.75	0.1086	0.1057	0.0723	0.0215	0.0230	0.0098	0.1086
911	2.75	0.1049	0.1016	0.0693	0.0220	0.0232	0.0083	0.1049
914	2.75	0.0975	0.0948	0.0621	0.0167	0.0182	0.0076	0.0975
917	2.75	0.0958	0.0960	0.0624	0.0166	0.0185	0.0093	0.0960
920	2.75	0.0981	0.1012	0.0666	0.0210	0.0229	0.0140	0.1012
923	2.75	0.0997	0.1031	0.0680	0.0211	0.0230	0.0141	0.1031
544	24.75	0.4971	0.4939	0.5069	0.4600	0.4635	0.4382	0.5069
606	24.75	1.0578	1.0545	1.1389	1.1680	1.1786	1.1536	1.1786
627	24.75	1.1597	1.1651	1.2680	1.2713	1.2706	1.2586	1.2713
630	24.75	1.2486	1.2121	1.3043	1.3068	1.2897	1.2586	1.3068
633	24.75	0.7923	0.7711	0.8695	0.8700	0.8391	0.8153	0.8700
636	24.75	0.5105	0.5017	0.5243	0.4580	0.4545	0.4220	0.5243
4965	24.75	0.3714	0.3767	0.4370	0.4847	0.4890	0.4873	0.4890
4968	24.75	0.6297	0.6551	0.7422	0.8236	0.8312	0.8340	0.8340
5035	24.75	0.6213	0.6423	0.7047	0.7915	0.8004	0.8114	0.8114
570	33.5	0.6528	0.6464	0.6879	0.6456	0.6461	0.6095	0.6879
753	33.5	0.6367	0.6307	0.6390	0.6103	0.6117	0.5769	0.6390
1411	33.5	0.6499	0.6450	0.6740	0.6445	0.6447	0.6122	0.6740
2657	33.5	0.6172	0.6120	0.6403	0.6164	0.6156	0.5868	0.6403
2738	33.5	0.5843	0.5800	0.5843	0.5698	0.5614	0.5341	0.5843

Table A.3-2 Maximum Relative Displacement in Y Direction (North-South) Relative to Free-Field Input Motion (Uncracked Case)

(Sheet 2 of 2)

Node No.	Elevation (feet)	Maximum Nodal Displacements (inch)						
		Subsurface Profile						Enveloping Maximum
		270-200	270-500	560-500	900-100	900-200	2032-100	
5039	33.5	0.4413	0.4593	0.4233	0.4559	0.4538	0.4424	0.4593
5042	33.5	0.4151	0.4312	0.3970	0.4458	0.4434	0.4332	0.4458
5045	33.5	0.3484	0.3580	0.3588	0.4038	0.4013	0.3961	0.4038
5048	33.5	0.3051	0.3181	0.3746	0.4070	0.4096	0.4068	0.4096
5080	33.5	0.3172	0.3278	0.3888	0.4245	0.4268	0.4266	0.4268
542	60.5	1.3303	1.3236	1.3956	1.3832	1.3800	1.3251	1.3956
573	60.5	1.2783	1.2671	1.3673	1.3462	1.3466	1.2856	1.3673
605	60.5	2.0327	1.9995	2.2832	2.3784	2.3757	2.3011	2.3784
626	60.5	2.1826	2.1370	2.2777	2.2922	2.2784	2.2182	2.2922
629	60.5	2.1442	2.1137	2.3061	2.2702	2.2689	2.2110	2.3061
632	60.5	1.3337	1.3070	1.4288	1.6217	1.6440	1.6320	1.6440
635	60.5	1.1503	1.1419	1.2540	1.2145	1.2100	1.1621	1.2540
755	60.5	1.3366	1.3257	1.4544	1.4415	1.4403	1.3794	1.4544
1421	60.5	1.3388	1.3281	1.4655	1.4547	1.4568	1.3958	1.4655
2659	60.5	1.2039	1.1938	1.2895	1.2828	1.2792	1.2281	1.2895
2740	60.5	1.0916	1.0821	1.1375	1.1314	1.1254	1.0755	1.1375
4964	63.5	0.8985	0.9103	1.0509	1.1677	1.1821	1.1816	1.1821
4967	63.5	0.9479	0.9747	1.0567	1.1853	1.1909	1.1915	1.1915
5034	63.5	0.9406	0.9591	1.0345	1.1241	1.1238	1.0928	1.1241
5037	63.5	0.8733	0.8891	0.9660	1.0474	1.0483	1.0194	1.0483
5041	63.5	0.8235	0.8384	0.9170	0.9957	0.9955	0.9699	0.9957
5044	63.5	0.7362	0.7462	0.8201	0.8933	0.8971	0.8779	0.8971
5047	63.5	0.6521	0.6625	0.7645	0.8531	0.8577	0.8558	0.8577
5079	63.5	0.6521	0.6681	0.7740	0.8648	0.8689	0.8711	0.8711
574	87.6667	1.6805	1.6519	1.8562	1.8349	1.8375	1.7559	1.8562
756	87.6667	1.7007	1.6623	1.8804	1.8573	1.8614	1.7800	1.8804
1422	87.6667	1.6625	1.6477	1.8418	1.8220	1.8230	1.7426	1.8418
2660	87.6667	1.5932	1.5819	1.7166	1.7068	1.7020	1.6226	1.7166
2741	87.6667	1.5022	1.4883	1.5759	1.5718	1.5602	1.4875	1.5759
661	169.417	3.1874	3.1200	3.4071	3.5706	3.5181	3.3813	3.5706
745	169.417	2.8611	2.7970	3.1991	3.2441	3.2395	3.0975	3.2441
3164	169.417	2.9323	2.8663	3.2796	3.3848	3.3825	3.2962	3.3848
3210	169.417	2.9078	2.8540	3.1050	3.0508	3.0109	2.8713	3.1050

Table A.3-3 Summary of Governing Subsurface Profiles for Maximum Relative Displacement in X (East-West) and Y (North-South) Directions

(Sheet 1 of 2)

Node No.	Elevation (feet)	Governing Subsurface Profile	
		East-West Direction	North-South Direction
290	2.75	270-200	270-500
338	2.75	270-200	270-200
386	2.75	270-200	270-200
389	2.75	270-200	270-200
392	2.75	270-200	270-200
395	2.75	270-200	270-500
398	2.75	270-200	270-500
401	2.75	270-200	270-500
473	2.75	270-200	270-200
560	2.75	270-200	270-500
676	2.75	270-200	270-500
792	2.75	270-200	270-500
879	2.75	270-200	270-500
908	2.75	270-500	270-200
911	2.75	270-200	270-200
914	2.75	270-200	270-200
917	2.75	270-200	270-500
920	2.75	270-200	270-500
923	2.75	270-200	270-500
544	24.75	900-100	560-500
606	24.75	900-100	900-200
627	24.75	900-100	900-100
630	24.75	900-100	900-100
633	24.75	900-100	900-100
636	24.75	900-100	560-500
4965	24.75	900-200	900-200
4968	24.75	900-200	2032-100
5035	24.75	900-200	2032-100
570	33.5	270-200	560-500
753	33.5	560-500	560-500
1411	33.5	560-500	560-500
2657	33.5	270-200	560-500
2738	33.5	560-500	270-200

Table A.3-3 Summary of Governing Subsurface Profiles for Maximum Relative Displacement in X (East-West) and Y (North-South) Directions

(Sheet 2 of 2)

Node No.	Elevation (feet)	Governing Subsurface Profile	
		East-West Direction	North-South Direction
5039	33.5	270-500	270-500
5042	33.5	560-500	900-100
5045	33.5	900-200	900-100
5048	33.5	900-200	900-200
5080	33.5	270-500	900-200
542	60.5	900-200	560-500
573	60.5	270-200	560-500
605	60.5	900-200	900-100
626	60.5	560-500	900-100
629	60.5	560-500	560-500
632	60.5	560-500	900-200
635	60.5	560-500	560-500
755	60.5	560-500	560-500
1421	60.5	560-500	560-500
2659	60.5	2032-100	560-500
2740	60.5	560-500	560-500
4964	63.5	270-200	900-200
4967	63.5	270-200	2032-100
5034	63.5	270-200	900-100
5037	63.5	270-500	900-200
5041	63.5	900-200	900-100
5044	63.5	900-200	900-200
5047	63.5	900-200	900-200
5079	63.5	900-200	2032-100
574	87.6667	560-500	560-500
756	87.6667	560-500	560-500
1422	87.6667	560-500	560-500
2660	87.6667	270-200	560-500
2741	87.6667	2032-100	560-500
661	169.417	560-500	900-100
745	169.417	560-500	900-100
3164	169.417	900-200	900-100
3210	169.417	900-200	560-500

A.4.0 RESULTS OF T/B COMPLEX STABILITY EVALUATIONS

Table A.4-1 reports the calculated minimum factors of safety against seismic overturning for each soil profile for both the X (East-West) and Y (North-South) directions. Table A.4-2 reports the calculated maximum seismic bearing pressures and minimum contact area ratios for each soil profile.

Table A.4-1 Turbine Building and Electrical Room Minimum Overturning Factor of Safety for Each Subsurface Profile (Uncracked Case)

Subsurface Profile	Minimum Factor of Safety[1]	
	About the East-West Direction (X-axis)	About the North-South Direction (Y-axis)
270-200	1.6	1.5
270-500	1.6	1.5
560-500	1.5	1.3
900-100	1.4	1.3
900-200	1.4	1.3
2032-100	1.4	1.3

Notes:
(1) Factor of Safety rounded down to nearest tenth.

Table A.4-2 Turbine Building and Electrical Room Maximum Bearing Pressure and Minimum Contact Area Ratio for Each Subsurface Profile (Uncracked Case)

Subsurface Profile	Results Including Buoyancy Force		Results Excluding Buoyancy Force	
	Maximum Bearing Pressure (ksf)	Minimum Contact Area Ratio (%)	Maximum Bearing Pressure (ksf)	Minimum Contact Area Ratio (%)
270-200	7.3	84.1	9.2	98.4
270-500	7.2	84.5	9.1	98.6
560-500	7.2	75.3	8.8	97.7
900-100	7.4	75.0	9.0	97.6
900-200	7.3	74.4	8.9	97.6
2032-100	7.3	74.4	9.0	98.2